Commun. Comput. Phys.
doi: 10.4208/cicp.170310.251110a

Vol. **10**, No. 4, pp. 940-978
October 2011

Staggered Lagrangian Discretization Based on Cell-Centered Riemann Solver and Associated Hydrodynamics Scheme

Pierre-Henri Maire[1], Raphaël Loubère[2,*] and Pavel Váchal[3]

[1] *CEA-CESTA, BP 2, 33114, Le Barp, France.*
[2] *Institut de Mathématiques de Toulouse (IMT) Université Paul-Sabatier and CNRS, Toulouse, France.*
[3] *FNSPE, Czech Technical University (CTU) in Prague, Czech Republic.*

Received 17 March 2010; Accepted (in revised version) 25 November 2010

Available online 22 June 2011

Abstract. The aim of the present work is to develop a general formalism to derive staggered discretizations for Lagrangian hydrodynamics on two-dimensional unstructured grids. To this end, we make use of the compatible discretization that has been initially introduced by E. J. Caramana et al., in J. Comput. Phys., 146 (1998). Namely, momentum equation is discretized by means of subcell forces and specific internal energy equation is obtained using total energy conservation. The main contribution of this work lies in the fact that the subcell force is derived invoking Galilean invariance and thermodynamic consistency. That is, we deduce a general form of the sub-cell force so that a cell entropy inequality is satisfied. The subcell force writes as a pressure contribution plus a tensorial viscous contribution which is proportional to the difference between the nodal velocity and the cell-centered velocity. This cell-centered velocity is a supplementary degree of freedom that is solved by means of a cell-centered approximate Riemann solver. To satisfy the second law of thermodynamics, the local subcell tensor involved in the viscous part of the subcell force must be symmetric positive definite. This subcell tensor is the cornerstone of the scheme. One particular expression of this tensor is given. A high-order extension of this discretization is provided. Numerical tests are presented in order to assess the efficiency of this approach. The results obtained for various representative configurations of one and two-dimensional compressible fluid flows show the robustness and the accuracy of this scheme.

AMS subject classifications: 52B10, 65D18, 68U05, 68U07

Key words: Lagrangian scheme, Riemann solver, artificial viscosity, hydrodynamics, compressible flow.

*Corresponding author. *Email addresses:* maire@celia.u-bordeaux1.fr (P.-H. Maire), raphael.loubere@math.univ-toulouse.fr (R. Loubère), vachal@galileo.fjfi.cvut.cz (P. Váchal)

1 Introduction

In Lagrangian hydrodynamics methods, a computational cell moves with the flow velocity. In practice, this means that the cell vertices move with a computed velocity, the cell faces being uniquely specified by the vertex positions. Thus, Lagrangian methods can capture contact discontinuity sharply in multi-material fluid flows. However, in the Lagrangian framework, one has to discretize not only the gas dynamics equations but also the vertex motion in order to move the mesh. Moreover, the numerical fluxes of the physical conservation laws must be determined in a compatible way with the vertex velocity so that the geometric conservation law (GCL) is satisfied, namely the rate of change of a Lagrangian volume has to be computed coherently with the node motion. This critical requirement is the cornerstone of any Lagrangian multi-dimensional scheme.

The most natural way to solve this problem employs a staggered discretization in which position, velocity and kinetic energy are centered at points, while thermodynamic variables (density, pressure and specific internal energy) are defined within cells. The dissipation of kinetic energy into internal energy through shock waves is ensured by an artificial viscosity term. Since the seminal works of von Neumann and Richtmyer [33], and Wilkins [34], many developments have been made in order to improve the accuracy and the robustness of staggered hydrodynamics [8, 11, 12]. More specifically, the construction of a compatible staggered discretization leads to a scheme that conserves total energy in a rigorous manner [9, 10].

An alternative to the previous discretizations is to derive a Lagrangian scheme based on the Godunov method [18]. In the Godunov-type method approach, all conserved quantities, including momentum, and hence cell velocity, are cell-centered. The cell-face quantities, including a face-normal component of the velocity, are available from the solution of an approximate Riemann problem at each cell face. However, it remains to determine the vertex velocity in order to move the mesh. In the early work [1] the flux computation was not compatible with the node displacement, and hence the GCL was not satisfied. This incompatibility generated additional spurious components in the vertex velocity field whose correction required expensive treatment [17]. An important achievement concerning the compatibility between flux discretization and vertex velocity computation has been introduced in [15,27]. In these papers, the authors present schemes in which the interface fluxes and the node velocity are computed coherently thanks to an approximate Riemann solver located at the nodes. This original approach leads to first-order conservative schemes which satisfy a local semi-discrete entropy inequality. The multi-dimensional high-order extension of these schemes are developed in [13,25,26,28].

The staggered discretization of variables (kinematic variables located at nodes, thermodynamic ones at cell centers) allows the scheme to fulfill naturally the GCL compatibility requirement and at the same time to construct a discrete divergence operator. The discretizations of momentum and specific internal energy are derived from each other by use of the important concepts of subcell mass, subcell force and total energy conservation [10]. This compatible hydrodynamics algorithm is thus designed to conserve

momentum and total energy exactly in discrete form by using the adjointness property of the discrete gradient and divergence operators. The dissipation of kinetic energy into internal energy through shock waves is ensured by means of an artificial viscosity which can be edge based [12] or tensorial [8]. This mechanism leads to a dissipation that is coherent with the second law of thermodynamics. The subcell pressure method is also used for control of hourglass type motion [11]. Finally, the time integration method is a predictor-corrector technique which is detailed in [10]. The extension of this compatible Lagrangian hydrodynamics algorithm to unstructured grids, where each zone is a polygon with an arbitrary number of sides, has been presented in [9].

Adopting the important concept of the subcells, we are proceeding in the opposite direction than designers of the staggered methods: instead of postulating a form of the artificial viscosity force and the anti-hourglass force, the force is derived from first principles by requiring Galilean invariance and thermodynamic consistency. In other words, if staggered and cell-centered approaches are two paths to the same objective, then the artificial viscosity term (explicit or implicit) should result as a difference of the cell-centered approach (which naturally contains dissipation on shocks) and the staggered approach with the artificial viscosity turned off. The hope is that such artificial viscosity term (if it exists) will be closely related to physical viscosity and thus will improve the method's performance (for example in [8], the authors blame the jets along Cartesian axes in Noh problem on the insufficiency of edge-based artificial viscosity model).

In Godunov methods, the dissipation of kinetic energy into internal energy is provided by solution of a Riemann problem. Our aim here is to use the same mechanism in the framework of a staggered scheme. The solution of the cell-centered Riemann problem provides an approximation of the cell-centered velocity $\boldsymbol{u}_c$, which will then be used to define the viscous part of the subcell force. This formulation allows a straightforward extension to second order in space by constructing linear velocity vector field approximation with frame invariant limitation, applicable on any mesh structure. At this point let us stress that careful and sensitive vector limitation is a key issue to effective exploitation of the improvement gained by frame invariant higher order extension, which is however a fact not always reflected in the design of existing methods. For example, dimensionally split limiters depend on Cartesian framework and thus fail to preserve rotational symmetry. As for temporal integration, we achieve second order in time by employing the predictor-corrector approach.

In the simplest case the resulting viscosity force can be expressed with the help of a symmetric positive definite matrix M_{cp}, so that the thermodynamic consistency is satisfied automatically by the viscous term $\mathsf{M}_{cp}\left(\boldsymbol{u}_c-\boldsymbol{u}_p\right)$. In particular, we are adopting the approximate Riemann solver by Dukowicz [16], which is based on the two-shock approximation and gives a viscous term not far from the classical formula by Kuropatenko [20, 34]. It turns out that a similar term (differing only in particular form of tensor M_{cp}) is implicitly contained in some cell-centered schemes such as [15].

Our method can be viewed as an extension of the work by Christensen [14], who noticed that under certain assumptions the staggered Lagrangian schemes with artificial

viscosity can be written in the same form as Godunov's scheme with HLL approximate Riemann solver and stressed the potential synergy of both approaches (e.g., higher-order extension of simple staggered scheme by techniques typically used in the Godunov community, such as TVD limiters). At this point let us remark, that the relationship between staggered Lagrangian and cell-centered Godunov methods from the viewpoint of shock-capturing mechanism has been discussed already in earlier works, e.g., by Wilkins [35] or Dukowicz [16]. Another step towards "bridging the Lagrange-Godunov conceptual gap" was done by Luttwak and Falcovitz [24], who also use a Riemann solver to provide necessary dissipation at shocks in the staggered scheme. The suggested SMG/Q method computes cell-centered velocity gradient to define a principal direction for limiter and shock detector in one. This approach is claimed to be superior to Christensen's split Q in multiple dimensions while being similar to it in the one-dimensional case. Moreover it can be used on structured as well as unstructured meshes. However, the authors themselves are still not happy with the uniaxial formulation of viscosity. Finally let us mention that since linking Godunov with staggered methods is an active research area, this topic was recently also investigated by Burbeau-Augoula [6], who introduced an additional degree of freedom by piecewise constant interpolation of selected variables on primary resp. dual cells. This establishes a connection between cell-centered and staggered formulation. The extra degree of freedom is then coupled to the nodal velocity by defining two half-Riemann problems per edge, which are subsequently treated by the HLL approximate Riemann solver. Assigning each half of the edge the velocity of its corresponding node (endpoint) provides a first order scheme. Besides other issues, on the way to frame invariant higher order extension of this method the strategy of proper limitation must be addressed.

The paper is organized as follows. First the governing equations and notations are stated. The compatible discretization is then derived from first principles. The fourth section deals with the definition of the fundamental object named subcell force. This previous derivation shows the necessity of the introduction of a cell-centered velocity as a new degree of freedom. This velocity is then determined in the fifth section through the use of a cell-centered approximate Riemann solver. High-order extension in space is also provided. The sixth section presents the high-order time discretization. In the last section, numerical results are proposed to assess the validity of this approach. Conclusions and perspectives are finally drawn.

2 Governing equations and notations

2.1 Governing equations

In Lagrangian framework, the two-dimensional gas dynamics equations write

$$\rho \frac{d}{dt}\left(\frac{1}{\rho}\right) - \nabla \cdot \boldsymbol{U} = 0, \tag{2.1a}$$

$$\rho\frac{d}{dt}\boldsymbol{U}+\boldsymbol{\nabla}P=\boldsymbol{0}, \tag{2.1b}$$

$$\rho\frac{d}{dt}E+\nabla\cdot(P\boldsymbol{U})=0, \tag{2.1c}$$

where ρ is the density, $\boldsymbol{U}$ the velocity, E the specific total energy and $\frac{d}{dt}$ denotes the material derivative. The first equation expresses the volume conservation equation, whereas the second and third ones are the momentum and total energy conservation equations. Volume conservation equation is often referred to as the Geometric Conservation Law (GCL). The previous system is equipped with a thermodynamics closure, Equation of State (EOS), $P=P(\rho,\varepsilon)$, where the specific internal energy is given by $\varepsilon=E-\boldsymbol{U}^2/2$. Note that for smooth solutions energy equation can be rewritten as

$$\rho\frac{d}{dt}\varepsilon+P\nabla\cdot\boldsymbol{U}=0, \tag{2.2}$$

and, substituting volume equation yields

$$\rho\frac{d}{dt}\varepsilon+P\rho\frac{d}{dt}\left(\frac{1}{\rho}\right)=0. \tag{2.3}$$

Recalling Gibbs relation for temperature T and specific entropy S: $TdS=d\varepsilon+Pd(\frac{1}{\rho})$, and the second law of thermodynamics, namely $T\frac{dS}{dt}\geq 0$, implies that for non-smooth flows the following relation holds:

$$\rho\frac{d}{dt}\varepsilon+P\nabla\cdot\boldsymbol{U}\geq 0. \tag{2.4}$$

As a consequence, internal energy equation can be viewed as an entropy evolution equation since

$$\rho\frac{d}{dt}\varepsilon+P\rho\frac{d}{dt}\left(\frac{1}{\rho}\right)\geq 0. \tag{2.5}$$

The previous System (2.1a)-(2.1c) can therefore be rewritten as a non-conservative system by replacing the energy equation by (2.4). The last equations are the trajectory equations

$$\frac{d\boldsymbol{X}}{dt}=\boldsymbol{U}(\boldsymbol{X}(t),t),\qquad \boldsymbol{X}(0)=\boldsymbol{x}, \tag{2.6}$$

expressing the Lagrangian motion of any point initially located at position $\boldsymbol{x}$.

2.2 Notations

We use a staggered placement of variables in which position and velocity are defined at grid points while thermodynamic variables are located at cell centers, refer to Fig. 1. An

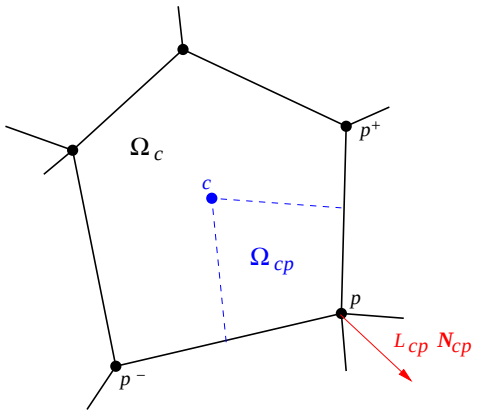

Figure 1: Fragment of a polygonal grid. Position and velocity are defined at grid points while thermodynamic variables are located at cell centers. A polygonal cell, Ω_c, is subdivided into subcells Ω_{cp}. Points are denoted by subscript p and ordered counterclockwise: p^-, p, p^+.

unstructured grid consisting of a collection of non-overlapping polygons is considered. Each polygonal cell is assigned a unique index c and is denoted Ω_c. Each vertex/point of the mesh is assigned a unique index p and we denote $\mathcal{C}(p)$ the set of cells sharing a particular vertex p. Each polygonal cell is subdivided into a set of subcells; each being uniquely defined by a pair of indices c and p and denoted Ω_{cp}. This subcell is constructed by connecting the cell center of Ω_c to the mid-points of cell edges impinging at point p. The union of subcells Ω_{cp} that share a particular vertex p allows to define the dual vertex-centered cell Ω_p related to point p with $\Omega_p = \bigcup_{c\in\mathcal{C}(p)} \Omega_{cp}$. Using the previous notation, we can define the primary grid $\bigcup_c \Omega_c$ and the dual grid $\bigcup_p \Omega_p$. The volumes of the primary and dual cells are functions of time t. Here, following [10], we make the fundamental assumption that the subcells are Lagrangian volumes. This means that the subcell mass m_{cp} is constant in time. Therefore, being given the initial density field $\rho^0(\boldsymbol{x})$ one deduces the initial mean density in cell c

$$\rho_c^0 = \int_{\Omega_c(0)} \frac{\rho^0(\boldsymbol{x})}{V_c^0} \mathrm{d}\boldsymbol{x}, \tag{2.7}$$

where V_c^0 is the volume of cell Ω_c at time $t=0$. Subcell mass is defined as $m_{cp} = \rho_c^0\ V_{cp}^0$, where V_{cp}^0 is the initial volume of subcell Ω_{cp}. By summation of Lagrangian subcell masses one defines Lagrangian cell/point masses as

$$m_c = \sum_{p\in\mathcal{P}(c)} m_{cp}, \qquad m_p = \sum_{c\in\mathcal{C}(p)} m_{cp}, \tag{2.8}$$

where $\mathcal{P}(c)$ is the set of counterclockwise ordered vertices of cell c. For a vertex p of cell Ω_c we denote its previous and next vertices by p^- and p^+.

3 Compatible discretization

We construct staggered Lagrangian schemes using the well known methodology of compatible discretization which has been presented in [4,7,10]. The cornerstone of this type of discretization is the subcell force that acts from subcell cp onto point p. In this approach, the discretization of the internal energy equation in terms of subcell forces is deduced from total energy conservation. Here, we fully derive a generic abstract form of the subcell force so that an entropy inequality is satisfied, which ensures that kinetic energy is dissipated into internal energy through shock waves. The subcell force writes as a pressure contribution plus a tensorial viscous contribution which is proportional to the difference between the vertex-centered and cell-centered velocities. The cell-centered velocity is a supplementary degree of freedom which is determined invoking the fundamental principle of Galilean invariance. To satisfy the second law of thermodynamics, the local subcell matrix involved in the viscous part of the subcell force must be symmetric positive definite. This matrix is the fundamental object that allows to properly define an artificial viscosity required to stabilize the scheme. We remark, that this new framework leads to a new form of artificial viscosity which is derived using first principle arguments.

3.1 Geometric conservation law (GCL)

Here, we use a discretization of the volume Eq. (2.1a) that is compatible with the GCL. By GCL compatibility we mean that we are deriving a discrete divergence operator for the volume equation by requiring consistency of the divergence of the velocity field with the time rate of change of volume of the cell, refer to [29]. By noticing that $m_c = \rho_c V_c$, where $\rho_c = \rho_c(t)$ and $V_c = V_c(t)$ are the cell density and volume, we can write

$$m_c \frac{d}{dt}\Big(\frac{1}{\rho_c}\Big) = \frac{d}{dt} V_c,$$

using the fact that the cell mass is constant in time. Moreover, remarking that the cell volume can be expressed as a function of the position vectors of its vertices as follows

$$V_c(t) = \sum_{p\in\mathcal{P}(c)} \frac{1}{2}\big(\boldsymbol{X}_p \times \boldsymbol{X}_{p^+}\big)\cdot \boldsymbol{e}_z,$$

where $\boldsymbol{e}_z$ is the unit vector of the canonical basis in z direction, we deduce that the time rate of change of the cell volume writes

$$\frac{d}{dt} V_c = \sum_{p\in\mathcal{P}(c)} \boldsymbol{\nabla}_{\boldsymbol{X}_p} V_c \cdot \frac{d}{dt}\boldsymbol{X}_p.$$

Here, we have simply applied the chain rule differentiation. Setting

$$\frac{d}{dt}\boldsymbol{X}_p = \boldsymbol{U}_p,$$

where $\boldsymbol{U}_p$ is the vertex velocity, we rewrite this last equation as

$$\frac{d}{dt}V_c - \sum_{p\in\mathcal{P}(c)} L_{cp}\boldsymbol{N}_{cp}\cdot\boldsymbol{U}_p = 0, \tag{3.1}$$

where $L_{cp}\boldsymbol{N}_{cp}$, with $\boldsymbol{N}_{cp}^2=1$, stands for the corner vector defined by $L_{cp}\boldsymbol{N}_{cp}=\boldsymbol{\nabla}_{\boldsymbol{X}_p}V_c$. This corner vector is a fundamental geometric object which is nothing but the gradient of the cell volume at point p. Its explicit expression in terms of points coordinates writes

$$L_{cp}\boldsymbol{N}_{cp}=\frac{1}{2}\begin{pmatrix} Y_{p^+}-Y_{p^-} \\ -(X_{p^+}-X_{p^-}) \end{pmatrix},$$

where (X_p,Y_p) denote the coordinate of the position vector $\boldsymbol{X}_p$. This kind of formalism is well known and has been used in staggered and cell-centered (free Lagrange) discretizations long time ago [29, 32]. We note that (3.1) is compatible with the discrete version of the trajectory equation (2.6)

$$\frac{d}{dt}\boldsymbol{X}_p=\boldsymbol{U}_p, \qquad \boldsymbol{X}_p(0)=\boldsymbol{x}_p.$$

This leads to a compatible definition of the discrete divergence operator over cell c as

$$(\nabla\cdot\boldsymbol{U})_c=\frac{1}{V_c}\sum_{p\in\mathcal{P}(c)} L_{cp}\boldsymbol{N}_{cp}\cdot\boldsymbol{U}_p. \tag{3.2}$$

We also emphasize that the corner vector $L_{cp}\boldsymbol{N}_{cp}$ satisfies the fundamental geometric identity

$$\sum_{p\in\mathcal{P}(c)} L_{cp}\boldsymbol{N}_{cp}=\boldsymbol{0}, \tag{3.3}$$

which is equivalent to the well known result that the summation of the outward normals to a closed polygonal contour is equal to zero.

Finally, we have obtained a compatible discretization of the volume equation (2.1a), which writes

$$m_c\frac{d}{dt}\left(\frac{1}{\rho_c}\right) - \sum_{p\in\mathcal{P}(c)} L_{cp}\boldsymbol{N}_{cp}\cdot\boldsymbol{U}_p = 0. \tag{3.4}$$

3.2 Momentum equation

The semi-discrete momentum equation over the dual cell Ω_p writes

$$m_p\frac{d}{dt}\boldsymbol{U}_p + \sum_{c\in\mathcal{C}(p)} \boldsymbol{F}_{cp}=\boldsymbol{0}. \tag{3.5}$$

Here, $\boldsymbol{F}_{cp}$ is the subcell force from cell c that acts on point p, which is defined by

$$\boldsymbol{F}_{cp} = \int_{\partial\Omega_p(t)\cap\Omega_c(t)} P\boldsymbol{N}\mathrm{d}l. \tag{3.6}$$

Momentum equation (3.5) is nothing but the Newton law applied to particle of mass m_p moving with velocity $\boldsymbol{U}_p$.

3.3 Specific internal energy equation

Here we derive a semi-discrete internal energy equation that ensures total energy conservation using the concept of subcell force, following the approach initially described in [10]. Let us introduce total kinetic energy and total internal energy

$$\mathcal{K}(t) = \sum_p \frac{1}{2} m_p \boldsymbol{U}_p^2(t), \qquad \mathcal{E}(t) = \sum_c m_c \varepsilon_c(t),$$

where ε_c is the cell-averaged specific internal energy. Total energy is then defined as $E(t)=\mathcal{K}(t)+\mathcal{E}(t)$. The conservation of total energy without taking into account boundary conditions simply writes

$$\frac{d}{dt}E = \frac{d}{dt}\mathcal{K} + \frac{d}{dt}\mathcal{E} = 0.$$

The substitution of kinetic and internal energies recalling that cell/point masses are Lagrangian objects, i.e., they not depend on time, yields

$$\frac{d}{dt}\mathcal{K} + \frac{d}{dt}\mathcal{E} = \sum_c m_c \frac{d}{dt}\varepsilon_c + \sum_p m_p \frac{d}{dt}\boldsymbol{U}_p \cdot \boldsymbol{U}_p.$$

Using the semi-discrete momentum equation (3.5) yields

$$\sum_c m_c \frac{d}{dt}\varepsilon_c - \sum_p \sum_{c\in\mathcal{C}(p)} \boldsymbol{F}_{cp}\cdot\boldsymbol{U}_p = 0,$$

interchanging the order in the double sum one finally gets

$$\sum_c \Big(m_c \frac{d}{dt}\varepsilon_c - \sum_{p\in\mathcal{P}(c)} \boldsymbol{F}_{cp}\cdot\boldsymbol{U}_p \Big) = 0. \tag{3.7}$$

A sufficient condition for total energy conservation is obtained by requiring the previous equation to hold in each cell c

$$m_c \frac{d}{dt}\varepsilon_c - \sum_{p\in\mathcal{P}(c)} \boldsymbol{F}_{cp}\cdot\boldsymbol{U}_p = 0. \tag{3.8}$$

Once the subcell force is known, then momentum and internal energy can be updated using Eqs. (3.5) and (3.8).

3.4 Summary of the compatible discretization

We summarize the semi-discrete equations that govern the time rate of change of the primary variables $(\frac{1}{\rho_c}, \boldsymbol{U}_p, \varepsilon_c)$:

$$
\begin{aligned}
&m_c \frac{d}{dt}\Big(\frac{1}{\rho_c}\Big) - \sum_{p\in\mathcal{P}(c)} L_{cp}\boldsymbol{N}_{cp}\cdot\boldsymbol{U}_p = 0,\\
&m_p \frac{d}{dt}\boldsymbol{U}_p + \sum_{c\in\mathcal{C}(p)} \boldsymbol{F}_{cp} = \boldsymbol{0},\\
&m_c \frac{d}{dt}\varepsilon_c - \sum_{p\in\mathcal{P}(c)} \boldsymbol{F}_{cp}\cdot\boldsymbol{U}_p = 0.
\end{aligned}
$$

We point out that the mesh motion is given by the trajectory equations

$$
\frac{d}{dt}\boldsymbol{X}_p = \boldsymbol{U}_p(\boldsymbol{X}_p(t),t), \qquad \boldsymbol{X}_p(0) = \boldsymbol{x}_p,
$$

which is compatible with the GCL. The thermodynamic closure is given by the equation of state which writes $P_c = P(\rho_c, \varepsilon_c)$. We emphasize that this subcell-based compatible discretization ensures total energy conservation regardless of the subcell force form. Now, it remains to determine the general form of this force so that our semi-discrete scheme fulfills, first, the principle of being Galilean invariant, second, the principle of being consistent with the second law of thermodynamics.

4 Definition of the subcell force

Here we provide a definition of the subcell force using Galilean invariance and thermodynamic consistency.

4.1 Galilean invariance

Galilean invariance is a principle of relativity which states that the fundamental laws of physics are the same in all inertial frames. It is one of the key requirements of many physical models adopted in theoretical and computational mechanics. To fulfill Galilean invariance, the previously derived specific internal energy equation (3.8) must remain unchanged under a uniform translation of frame. Let $\boldsymbol{A}$ denote the uniform translation velocity. Then Eq. (3.8) transforms into

$$
m_c \frac{d}{dt}\varepsilon_c - \sum_{p\in\mathcal{P}(c)} \boldsymbol{F}_{cp}\cdot(\boldsymbol{U}_p + \boldsymbol{A}) = 0.
$$

By substituting (3.8) into this last equation leads to

$$\sum_{p\in\mathcal{P}(c)} \boldsymbol{F}_{cp}\cdot\boldsymbol{A}=0,$$

which must hold for all vectors $\boldsymbol{A}$. Therefore, specific internal energy equation remains invariant under uniform translation if and only if

$$\sum_{p\in\mathcal{P}(c)} \boldsymbol{F}_{cp}=\boldsymbol{0}. \tag{4.1}$$

We note that this result has been already quoted in [4] page 576. This condition also implies total momentum conservation without taking into account boundary conditions. To demonstrate this, it suffices to time-differentiate the global momentum defined as $\boldsymbol{\mathcal{Q}}=\sum_p m_p\boldsymbol{U}_p$:

$$\begin{aligned}\frac{d}{dt}\boldsymbol{\mathcal{Q}}&=\sum_p m_p\frac{d}{dt}\boldsymbol{U}_p\\&=-\sum_p\sum_{c\in\mathcal{C}(p)}\boldsymbol{F}_{cp}\quad\text{(thanks to momentum equation)}\\&=-\sum_c\sum_{p\in\mathcal{P}(c)}\boldsymbol{F}_{cp}\quad\text{(by interchanging the double sums).}\end{aligned}$$

Thus, $\frac{d}{dt}\boldsymbol{\mathcal{Q}}=\boldsymbol{0}$ due to condition (4.1), which completes the proof.

A corollary of the Galilean invariance condition is that specific internal energy equation (3.8) can also be rewritten into

$$m_c\frac{d}{dt}\varepsilon_c-\sum_{p\in\mathcal{P}(c)}\boldsymbol{F}_{cp}\cdot(\boldsymbol{U}_p-\boldsymbol{U}_c)=0, \tag{4.2}$$

where $\boldsymbol{U}_c$ is a piecewise constant cell-centered velocity that remains to be determined.

4.2 Thermodynamic consistency

We investigate the thermodynamic consistency of our semi-discrete scheme by computing the time rate of change of entropy in cell c. Using Gibbs formula, one gets

$$m_cT_c\frac{d}{dt}S_c=m_c\Big[\frac{d}{dt}\varepsilon_c+P_c\frac{d}{dt}\Big(\frac{1}{\rho_c}\Big)\Big], \tag{4.3}$$

where S_c and T_c are the specific entropy and temperature of cell c. Substituting into (4.3) the specific internal energy equation (4.2) and the volume equation (3.4) yields

$$\begin{aligned}m_cT_c\frac{d}{dt}S_c&=\sum_{p\in\mathcal{P}(c)}\boldsymbol{F}_{cp}\cdot(\boldsymbol{U}_p-\boldsymbol{U}_c)+P_c\Big(\sum_{p\in\mathcal{P}(c)}L_{cp}\boldsymbol{N}_{cp}\cdot\boldsymbol{U}_p\Big)\\&=\sum_{p\in\mathcal{P}(c)}(\boldsymbol{F}_{cp}+L_{cp}P_c\boldsymbol{N}_{cp})\cdot(\boldsymbol{U}_p-\boldsymbol{U}_c).\end{aligned}$$

Here, we have used the geometric identity $\sum_{p\in\mathcal{P}(c)} L_{cp}\boldsymbol{N}_{cp}=\boldsymbol{0}$. To satisfy the second law of thermodynamics the right-hand side of the last equation must be positive. A sufficient condition to obtain this consists in setting

$$\boldsymbol{F}_{cp}=-L_{cp}P_c\boldsymbol{N}_{cp}+\mathsf{M}_{cp}(\boldsymbol{U}_p-\boldsymbol{U}_c), \tag{4.4}$$

where M_{cp} is a subcell-based matrix.

Given this form, several features of M_{cp} can be drawn:

1. *Dimensionality.* M_{cp} has dimension of density times velocity times length.
2. *Entropy inequality satisfaction.* M_{cp} is positive semidefinite, i.e., $\mathsf{M}_{cp}\boldsymbol{U}\cdot\boldsymbol{U}\geq 0, \forall \boldsymbol{U}\in\mathbb{R}^2$. By substituting (4.4) into (4.3), we obtain the entropy inequality satisfied by our semi-discrete scheme

$$m_cT_c\frac{\mathrm{d}}{\mathrm{d}t}S_c=\sum_{p\in\mathcal{P}(c)}\mathsf{M}_{cp}(\boldsymbol{U}_p-\boldsymbol{U}_c)\cdot(\boldsymbol{U}_p-\boldsymbol{U}_c)\geq 0, \tag{4.5}$$

   as the right-hand side is a positive semidefinite quadratic form.
3. *Galilean invariance.* M_{cp} is compatible with the principle of Galilean invariance: in a nutshell, M_{cp} must be invariant w.r.t. translation and transform as $\mathcal{R}\mathsf{M}_{cp}\mathcal{R}^t$ for a rigid rotation $\mathcal{R}$.
4. *Symmetry.* M_{cp} is symmetric, i.e., $\mathsf{M}_{cp}^t=\mathsf{M}_{cp}$.
5. *Locality.* M_{cp} is a locally defined matrix: the physical and geometric quantities involved in M_{cp} must be local in a neighborhood of the current subcell.

We remark that entropy production (4.5) within cell c is directly governed by the subcell matrix M_{cp} and the velocity jump between the nodal and the cell-centered velocity which still remains to be determined. This is the main topic of next section.

5 Cell-centered velocity computation

Using the previously derived generic form of the subcell force and the Galilean invariance condition, we develop a cell-centered solver to compute the cell-centered velocity.

5.1 Abstract formulation

Substituting the subcell force expression,

$$\boldsymbol{F}_{cp}=-L_{cp}P_c\boldsymbol{N}_{cp}+\mathsf{M}_{cp}(\boldsymbol{U}_p-\boldsymbol{U}_c),$$

into the Galilean invariance condition, $\sum_{p\in\mathcal{P}(c)}\boldsymbol{F}_{cp}=\boldsymbol{0}$, leads to the following system satisfied by the cell-centered velocity $\boldsymbol{U}_c$,

$$\mathsf{M}_c\boldsymbol{U}_c=\sum_{p\in\mathcal{P}(c)}\mathsf{M}_{cp}\boldsymbol{U}_p, \tag{5.1}$$

where $\mathsf{M}_c=\sum_{p\in\mathcal{P}(c)}\mathsf{M}_{cp}$ is a symmetric positive definite matrix. Once the definition of the subcell matrix M_{cp} is known, one can solve the previous system to get a unique expression of the cell-centered velocity. We shall see in the next paragraph one example of such a solver.

5.2 Cell-centered approximate Riemann solver

By analogy with the node-centered approximate Riemann solver introduced in the context of cell-centered Lagrangian discretization [26], we present one cell-centered approximate Riemann solver. This solver allows to determine one particular form of the subcell matrix M_{cp}. To this end, let us introduce two pressures at the cell center per subcell denoted by Π^-_{cp}, Π^+_{cp}. These pressures are related to the normals $\boldsymbol{N}^+_{cp}$, $\boldsymbol{N}^-_{cp}$ which are the unit outward normals to the subcell boundaries inside the cell, refer to Fig. 2. The subcell force is then defined as

$$\boldsymbol{F}_{cp}=L^-_{cp}\Pi^-_{cp}\boldsymbol{N}^-_{cp}+L^+_{cp}\Pi^+_{cp}\boldsymbol{N}^+_{cp}. \tag{5.2}$$

The cell-centered pressures are obtained by means of the half-Riemann problems

$$P_c-\Pi^-_{cp}=Z^-_{cp}\left(\boldsymbol{U}_c-\boldsymbol{U}_p\right)\cdot\boldsymbol{N}^-_{cp}, \tag{5.3a}$$

$$P_c-\Pi^+_{cp}=Z^+_{cp}\left(\boldsymbol{U}_c-\boldsymbol{U}_p\right)\cdot\boldsymbol{N}^+_{cp}, \tag{5.3b}$$

where Z^-_{cp}, Z^+_{cp} denote the swept mass fluxes, and $\boldsymbol{U}_c$ is the cell-centered velocity which remains to be computed. The swept mass fluxes, Z^-_{cp}, Z^+_{cp}, are defined following Dukowicz [16] as

$$Z^-_{cp}=\rho_c\left[\sigma_c+c_Q\Gamma_c|(\boldsymbol{U}_c-\boldsymbol{U}_p)\cdot\boldsymbol{N}^-_{cp}|\right],\qquad Z^+_{cp}=\rho_c\left[\sigma_c+c_Q\Gamma_c|(\boldsymbol{U}_c-\boldsymbol{U}_p)\cdot\boldsymbol{N}^+_{cp}|\right]. \tag{5.4}$$

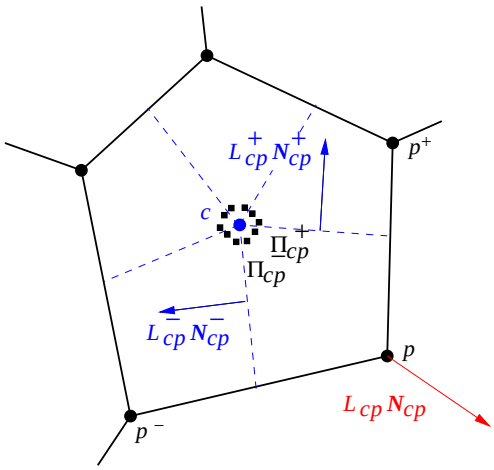

Figure 2: Notation used in the cell-centered Riemann solver. Two pressures per subcell (■) are introduced at the cell center: Π^+_{cp}, Π^-_{cp}. They are related to the outward normal vectors $L^+_{cp}\boldsymbol{N}^+_{cp}$, $L^-_{cp}\boldsymbol{N}^-_{cp}$. In total, $2|\mathcal{P}(c)|$ pressures are introduced within cell Ω_c.

Here, σ_c is the isentropic sound speed, c_Q a user-defined parameter (set to 1 in our simulations) and Γ_c a material dependent coefficient, which for a γ gas law is defined by

$$\Gamma_c = \begin{cases} \dfrac{\gamma+1}{2}, & \text{if } (\nabla\cdot\boldsymbol{U})_{cp} < 0, \\ 0, & \text{if } (\nabla\cdot\boldsymbol{U})_{cp} \geq 0, \end{cases} \tag{5.5}$$

where

$$(\nabla\cdot\boldsymbol{U})_{cp} = -\frac{1}{V_{cp}} L_{cp}\boldsymbol{N}_{cp}\cdot(\boldsymbol{U}_c - \boldsymbol{U}_p)$$

is the subcell contribution to the velocity divergence. In case of rarefaction wave, we recover the acoustic approximation whereas in case of shock wave we get the well known two-shock approximation.

Using (5.3) the subcell force is rewritten

$$\boldsymbol{F}_{cp} = \left(L^-_{cp}\boldsymbol{N}^-_{cp} + L^+_{cp}\boldsymbol{N}^+_{cp}\right)P_c + \mathsf{M}_{cp}\left(\boldsymbol{U}_p - \boldsymbol{U}_c\right), \tag{5.6}$$

where

$$\mathsf{M}_{cp} = Z^-_{cp}L^-_{cp}(\boldsymbol{N}^-_{cp}\otimes\boldsymbol{N}^-_{cp}) + Z^+_{cp}L^+_{cp}(\boldsymbol{N}^+_{cp}\otimes\boldsymbol{N}^+_{cp}) \tag{5.7}$$

is a 2×2 symmetric positive definite matrix. Noticing that the subcell contour is closed, we deduce that $L^-_{cp}\boldsymbol{N}^-_{cp} + L^+_{cp}\boldsymbol{N}^+_{cp} = -L_{cp}\boldsymbol{N}_{cp}$. Finally, the subcell force writes

$$\boldsymbol{F}_{cp} = -L_{cp}P_c\boldsymbol{N}_{cp} + \mathsf{M}_{cp}\left(\boldsymbol{U}_p - \boldsymbol{U}_c\right),$$

where the subcell matrix is given by (5.7). We emphasize that we have recovered the generic form of the subcell force which has been previously derived. Moreover, we have given a particular expression of the subcell matrix which is directly linked to the half-Riemann invariants (5.3). Finally, the cell-centered velocity $\boldsymbol{U}_c$ is obtained by solving the system $\mathsf{M}_c\boldsymbol{U}_c = \sum_{p\in\mathcal{P}(c)}\mathsf{M}_{cp}\boldsymbol{U}_p$, recalling that $\mathsf{M}_c = \sum_{p\in\mathcal{P}(c)}\mathsf{M}_{cp}$ and that M_{cp} is given by (5.7). We note that M_c is symmetric positive definite which ensures its invertibility. We remark that this system is non-linear due to the dependency of the swept mass flux on the cell-centered velocity. This non-linear system can be solved using an iterative procedure such as fixed point or Newton algorithms. In practice, few iterations are needed to reach convergence. Once the cell-centered velocity is known, the subcell force is deduced from Eq. (4.4). The present cell-centered approximate Riemann solver can be viewed as a two-dimensional extension of the work initiated by Christensen in one-dimensional framework [14].

5.3 High-order extension

The previously defined cell-centered approximate Riemann solver utilizes piecewise constant nodal velocities defined over the subcells of a given cell. In this sense, this leads to a first-order approximation of the cell-centered velocity. To get a more accurate approximation, we construct a piecewise linear representation of the nodal velocity field to feed the cell-centered solver with the extrapolated velocity at the cell center.

5.3.1 Piecewise linear reconstruction of the velocity field

First, we introduce a piecewise linear representation of the velocity field over the dual grid by setting

$$\boldsymbol{u}_p(\boldsymbol{X}) = \boldsymbol{u}_p + \nabla \boldsymbol{u}_p \cdot (\boldsymbol{X} - \boldsymbol{X}_p), \tag{5.8}$$

where $\nabla \boldsymbol{u}_p$ is the constant velocity tensor gradient over the dual cell Ω_p. To compute it we use a classical least squares approach by solving the following minimization problem

$$\nabla \boldsymbol{u}_p = \text{argmin} \sum_{q \in \mathcal{N}(p)} \left[(\boldsymbol{u}_q - \boldsymbol{u}_p) - \nabla \boldsymbol{u}_p (\boldsymbol{X}_q - \boldsymbol{X}_p) \right]^2, \tag{5.9}$$

where $\mathcal{N}(p)$ is the set of neighbor vertices of vertex p. The solution of this minimization problem reads

$$\nabla \boldsymbol{u}_p = \mathsf{M}_p^{-1} \sum_{q \in \mathcal{N}(p)} (\boldsymbol{u}_q - \boldsymbol{u}_p) \otimes (\boldsymbol{X}_q - \boldsymbol{X}_p), \tag{5.10}$$

where matrix M_p is the symmetric positive definite matrix

$$\mathsf{M}_p = \sum_{q \in \mathcal{N}(p)} (\boldsymbol{X}_q - \boldsymbol{X}_p) \otimes (\boldsymbol{X}_q - \boldsymbol{X}_p). \tag{5.11}$$

We emphasize that this least squares approach is valid for any type of unstructured grid and preserves linear velocity field.

5.3.2 Frame invariant tensorial limitation for a vector field

Monotonicity is achieved thanks to a modification of the classical Barth-Jespersen slope limiter [2,3]. For vectors, limiting is usually applied separately to each component. However, such a procedure is frame dependent and thus leads to rotational symmetry distortion. Namely, component limiters do not preserve symmetry since a rotation of the coordinate axis produces different results. This drawback is crucial in the framework of Lagrangian hydrodynamics since we are dealing with moving mesh discretizations which are particularly sensitive about symmetry loss. To correct this flaw, we have to construct a limiting procedure which is frame invariant for vectors. One possible choice is to use the Vector Image Polygon (VIP) methodology derived in [23]. This method consists in constructing the VIP as the convex hull of the vector-space points corresponding to the neighbor vectors. If a slope-extrapolated vector lies inside the VIP, the slope is monotonicity preserving, otherwise slope limiting is required. On the other hand, the slope is set to zero by analogy with the scalar limitation. Here we develop an original procedure to perform a limitation of vector field which preserves rotational symmetry. To define a limiter for the velocity tensor gradient, we define in each dual cell Ω_p a local

orthonormal basis $(\boldsymbol{\xi}_p^{\parallel},\boldsymbol{\xi}_p^{\perp})$ which is assumed to be frame independent. Let us define the coordinates of the vectors $\boldsymbol{\xi}_p^{\parallel}$ and $\boldsymbol{\xi}_p^{\perp}$ in the canonical basis by setting

$$\boldsymbol{\xi}_p^{\parallel}=\begin{pmatrix}\xi_x\\ \xi_y\end{pmatrix},\qquad \boldsymbol{\xi}_p^{\perp}=\begin{pmatrix}-\xi_y\\ \xi_x\end{pmatrix},$$

where $\xi_x^2+\xi_y^2=1$ so that $(\boldsymbol{\xi}_p^{\parallel},\boldsymbol{\xi}_p^{\perp})$ is a direct orthonormal basis. Thus the transformation matrix from the canonical basis to the local basis reads

$$\mathsf{A}_p=\begin{pmatrix}\xi_x & \xi_y\\ -\xi_y & \xi_x\end{pmatrix}.$$

The transformation of the nodal velocity $\boldsymbol{U}_p$ to the local coordinates is

$$\boldsymbol{W}_p=\begin{pmatrix}W_p^{\parallel}\\ W_p^{\perp}\end{pmatrix}=\mathsf{A}_p\boldsymbol{U}_p=\begin{pmatrix}\boldsymbol{\xi}_p^{\parallel}\cdot\boldsymbol{U}_p\\ \boldsymbol{\xi}_p^{\perp}\cdot\boldsymbol{U}_p\end{pmatrix}. \tag{5.12}$$

Then we find the minimum and maximum value from projections of neighboring nodes' velocities into new directions:

$$W_p^{\parallel,\max}=\max_{k\in\mathcal{N}(p)}\left(\boldsymbol{\xi}_p^{\parallel}\cdot\boldsymbol{U}_k\right),\qquad W_p^{\perp,\max}=\max_{k\in\mathcal{N}(p)}\left(\boldsymbol{\xi}_p^{\perp}\cdot\boldsymbol{U}_k\right), \tag{5.13a}$$

$$W_p^{\parallel,\min}=\min_{k\in\mathcal{N}(p)}\left(\boldsymbol{\xi}_p^{\parallel}\cdot\boldsymbol{U}_k\right),\qquad W_p^{\perp,\min}=\min_{k\in\mathcal{N}(p)}\left(\boldsymbol{\xi}_p^{\perp}\cdot\boldsymbol{U}_k\right), \tag{5.13b}$$

where $\mathcal{N}(p)$ is the set of neighbor points of current point p. Now consider cell $c\in\mathcal{C}(p)$ centered at $\boldsymbol{X}_c$. Using the unlimited piecewise linear representation of the velocity field, the extrapolated values of the velocity at point $\boldsymbol{X}_c$ are given by

$$\boldsymbol{U}_{p,c}\equiv\boldsymbol{U}_p(\boldsymbol{X}_c)=\boldsymbol{U}_p+\nabla\boldsymbol{U}_p\cdot\left(\boldsymbol{X}_c-\boldsymbol{X}_p\right), \tag{5.14}$$

and its transformation into the local basis $(\boldsymbol{\xi}_p^{\parallel},\boldsymbol{\xi}_p^{\perp})$ produces

$$\boldsymbol{W}_{p,c}=\begin{pmatrix}W_{p,c}^{\parallel}\\ W_{p,c}^{\perp}\end{pmatrix}=\mathsf{A}_p\boldsymbol{U}_{p,c}. \tag{5.15}$$

From these values we define

$$\phi_{p,c}^{\parallel}=\begin{cases}\mathcal{L}\left(\frac{W_p^{\parallel,\max}-W_p^{\parallel}}{W_{p,c}^{\parallel}-W_p^{\parallel}}\right), & \text{if } \left(W_{p,c}^{\parallel}-W_p^{\parallel}\right)>0,\\ \mathcal{L}\left(\frac{W_p^{\parallel,\min}-W_p^{\parallel}}{W_{p,c}^{\parallel}-W_p^{\parallel}}\right), & \text{if } \left(W_{p,c}^{\parallel}-W_p^{\parallel}\right)<0,\\ 1, & \text{if } \left(W_{p,c}^{\parallel}-W_p^{\parallel}\right)=0,\end{cases}$$

$$\phi_{p,c}^{\perp}=\begin{cases}\mathcal{L}\left(\frac{W_p^{\perp,\max}-W_p^{\perp}}{W_{p,c}^{\perp}-W_p^{\perp}}\right), & \text{if } \left(W_{p,c}^{\perp}-W_p^{\perp}\right)>0,\\ \mathcal{L}\left(\frac{W_p^{\perp,\min}-W_p^{\perp}}{W_{p,c}^{\perp}-W_p^{\perp}}\right), & \text{if } \left(W_{p,c}^{\perp}-W_p^{\perp}\right)<0,\\ 1, & \text{if } \left(W_{p,c}^{\perp}-W_p^{\perp}\right)=0,\end{cases}$$

where $\mathcal{L}(\alpha)$ is a suitable limiting functional such as

$$\mathcal{L}(\alpha)=\min(\alpha,1) \qquad \text{or} \qquad \mathcal{L}(\alpha)=(\alpha^2+2\alpha)(\alpha^2+\alpha+2)^{-1}.$$

The slope limiters for node p are finally defined by $\phi_p^{\parallel}$ and $\phi_p^{\perp}$ as

$$\phi_p^{\parallel}=\min_{c\in\mathcal{C}(p)}\phi_{p,c}^{\parallel}, \qquad \phi_p^{\perp}=\min_{c\in\mathcal{C}(p)}\phi_{p,c}^{\perp}.$$

This pair of limiters is transformed back into the Cartesian coordinates:

$$\Phi_p=\mathsf{A}_p^{-\mathbf{1}}\begin{pmatrix}\phi_p^{\parallel} & 0\\ 0 & \phi_p^{\perp}\end{pmatrix}\mathsf{A}_p=\begin{pmatrix}\xi_x^2\,\phi_p^{\parallel}+\xi_y^2\,\phi_p^{\perp} & \xi_x\,\xi_y\,\phi_p^{\parallel}-\xi_x\,\xi_y\,\phi_p^{\perp}\\ \xi_x\,\xi_y\,\phi_p^{\parallel}-\xi_x\,\xi_y\,\phi_p^{\perp} & \xi_y^2\,\phi_p^{\parallel}+\xi_x^2\,\phi_p^{\perp}\end{pmatrix}.$$

The limited tensor gradient is finally given by formula

$$\nabla\boldsymbol{u}_p^{\lim}=\Phi_p\nabla\boldsymbol{u}_p$$

and thus the limited velocity field reconstruction in the vicinity of node p is

$$\boldsymbol{u}_p(\boldsymbol{X})=\boldsymbol{u}_p+\nabla\boldsymbol{u}_p^{\lim}(\boldsymbol{X}-\boldsymbol{X}_p). \tag{5.16}$$

We claim that we have defined a tensorial limitation procedure for the velocity vector which is frame invariant and thus preserves rotational symmetry. In practice, we define the local basis utilizing the point velocity direction.

5.3.3 High-order cell-centered approximate Riemann solver

It consists in replacing the point velocity by its extrapolated value at cell center using the piecewise linear monotonic reconstruction. Namely, the system that solves $\boldsymbol{u}_c$ becomes

$$\mathsf{M}_c\boldsymbol{u}_c=\sum_{p\in\mathcal{N}(c)}\mathsf{M}_{cp}\boldsymbol{u}_p(\boldsymbol{X}_c),$$

where the swept mass fluxes entering the definition of the subcell matrices are also computed using the extrapolated velocity as

$$Z_{cp}^{\pm}=\rho_c\left[\sigma_c+c_Q\Gamma_c|(\boldsymbol{u}_c-\boldsymbol{u}_p(\boldsymbol{X}_c))\cdot\boldsymbol{N}_{cp}^{\pm}|\right].$$

The subcell force is modified accordingly:

$$\boldsymbol{F}_{cp}=-L_{cp}P_c\boldsymbol{N}_{cp}+\mathsf{M}_{cp}\big(\boldsymbol{u}_p(\boldsymbol{X}_c)-\boldsymbol{u}_c\big). \tag{5.17}$$

5.4 Subcell pressure based cell-centered Riemann solver

In Section 5.2, the cell-centered Riemann solver has been derived by considering a piecewise constant pressure inside the cell. Here we present a modification that takes into account the subcell pressures as in [11]. Indeed, the main assumption of the compatible formalism that has been used relies on the fact that subcells are Lagrangian volumes; namely subcell mass m_{cp} is constant in time. This main assumption leads to the following definition of subcell density

$$\rho_{cp}(t)=\frac{m_{cp}}{V_{cp}(t)}, \tag{5.18}$$

where $V_{cp}(t)$ is the subcell volume. To define the subcell pressure, $P_{cp}(t)$, we assume that the cell-centered specific internal energy is constant over the cell. Therefore, using the EOS, subcell pressure reads

$$P_{cp}(t)=P(\rho_{cp}(t),\varepsilon_c(t)). \tag{5.19}$$

To incorporate subcell pressure effects one substitutes P_{cp} into the half-Riemann problems that allow to define the subcell force. In other words, one replaces P_c in (5.3a)-(5.3b) by P_{cp} as follows

$$P_{cp}-\Pi^-_{cp}=Z^-_{cp}\big(\boldsymbol{u}_c-\boldsymbol{u}_p\big)\cdot\boldsymbol{N}^-_{cp}, \tag{5.20a}$$
$$P_{cp}-\Pi^+_{cp}=Z^+_{cp}\big(\boldsymbol{u}_c-\boldsymbol{u}_p\big)\cdot\boldsymbol{N}^+_{cp}. \tag{5.20b}$$

The swept mass fluxes are also modified by making use of the subcell density ρ_{cp} and sound speed σ_{cp} as

$$Z^{\pm}_{cp}=\rho_{cp}\big[\sigma_{cp}+c_{\mathrm{Q}}\Gamma_c|(\boldsymbol{u}_c-\boldsymbol{u}_p)\cdot\boldsymbol{N}^{\pm}_{cp}|\big].$$

The corresponding subcell force is modified accordingly

$$\boldsymbol{F}_{cp}=-L_{cp}P_{cp}\boldsymbol{N}_{cp}+\mathrm{M}_{cp}\big(\boldsymbol{u}_p-\boldsymbol{u}_c\big). \tag{5.21}$$

Then, the system that solves the cell-centered velocity rewrites as

$$\boldsymbol{u}_c=\mathrm{M}_c^{-1}\sum_{p\in\mathcal{P}(c)}\big(\mathrm{M}_{cp}\boldsymbol{u}_p-L_{cp}P_{cp}\boldsymbol{N}_{cp}\big). \tag{5.22}$$

Let us a give an interpretation of the two terms that determine the cell-centered velocity. The first term at the right-hand side is simply a weighted interpolation of nodal velocities at cell center, whereas the second corresponds to a discretization of the pressure gradient at cell center. This interpretation is easy to obtain by computing the pressure gradient integral over the cell as

$$\big(\boldsymbol{\nabla}P\big)_c=\frac{1}{V_c}\int_{\partial\Omega_c}P\boldsymbol{N}\mathrm{d}S. \tag{5.23}$$

Using the subcell decomposition, (5.23) rewrites

$$\left(\boldsymbol{\nabla} P\right)_c = \frac{1}{V_c} \sum_{p\in\mathcal{P}(c)} \int_{\partial\Omega_{cp}\cap\partial\Omega_c} P\boldsymbol{N}\,\mathrm{d}S = \frac{1}{V_c} \sum_{p\in\mathcal{P}(c)} L_{cp}P_{cp}\boldsymbol{N}_{cp}.$$

With this result the cell-centered velocity reads

$$\boldsymbol{u}_c = \sum_{p\in\mathcal{P}(c)} \mathsf{M}_c^{-1}\mathsf{M}_{cp}\boldsymbol{u}_p - V_c\mathsf{M}_c^{-1}\left(\boldsymbol{\nabla} P\right)_c. \tag{5.24}$$

This formula degenerates to the previous formula (5.1) in case of uniform subcell pressure over the cell. The extra pressure gradient term induced by the subcell pressures acts as a supplementary viscous term that is usually present in approximate Riemann solver. Namely, (5.24) can be viewed as a two-dimensional generalization of an acoustic Riemann solver. Indeed, in the case of a one-dimensional flow aligned with a rectangular grid, for $c_Q = 0$, one can show that the cell-centered velocity reduces to

$$\boldsymbol{u}_c = \Big(\frac{Z_l u_l + Z_r u_r}{Z_l + Z_r} - \frac{P_r - P_l}{Z_l + Z_r}\Big)\boldsymbol{e}_x,$$

where the subscripts l and r denote the left and right states of the one-dimensional Riemann problem on both sides of the interface.

We want to quote that the subcell pressure has been initially introduced in classical staggered discretization by Caramana and Shashkov [11] to control artificial grid distortions, such as the hourglass modes. Let us recall, that in the case of a logically rectangular grid, a quadrilateral cell has eight degrees of freedom. All but the two hourglass modes are physical, only for the hourglass modes does the subcell density differ from the cell density to which it belongs. The subcell pressure method uses this to calculate subcell forces that are proportional between the subcell and the cell pressures, and oppose the hourglass motion. In this approach, the subcell pressure force is defined as

$$\boldsymbol{F}_{cp}^{\Delta P} = L_{cp}(P_{cp} - P_c)\boldsymbol{N}_{cp} + \frac{1}{2}\left[\left(P_{cp} - P_{cp^-}\right)L_{cp}^-\boldsymbol{N}_{cp}^- + \left(P_{cp} - P_{cp^+}\right)L_{cp}^+\boldsymbol{N}_{cp}^+\right], \tag{5.25}$$

where P_{cp^-} and P_{cp^+} are the previous and next neighbor subcell pressures with respect to subcell cp.

6 Time discretization

The time discretization is performed with a classical two-step predictor-corrector scheme to gain second-order accuracy. Being given geometric quantities and physical variables at time t^n, we first predict the pressures that are later used in the corrector step to update physical and geometric variables. The full discretization in space and time is displayed in the following algorithm:

Predictor step

1. Piecewise monotonic linear reconstruction of the velocity field over the dual grid

$$\boldsymbol{U}_p^n(\boldsymbol{X}) = \boldsymbol{U}_p^n + \nabla \boldsymbol{U}_p^{\lim}(\boldsymbol{X} - \boldsymbol{X}_p^n).$$

2. Compute $\boldsymbol{U}_c^n$ with the high-order cell-centered Riemann solver

$$\boldsymbol{U}_c^n = \left(\mathsf{M}_c^n\right)^{-1} \sum_{p \in \mathcal{P}(c)} \left[-\left(L_{cp}\boldsymbol{N}_{cp}\right)^n P_{cp}^n + \mathsf{M}_{cp}^n \boldsymbol{U}_p^n(\boldsymbol{X}_c^n) \right].$$

3. Compute subcell forces

$$\boldsymbol{F}_{cp}^n = -\left(L_{cp}\boldsymbol{N}_{cp}\right)^n P_{cp}^n + \mathsf{M}_{cp}^n \left(\boldsymbol{U}_p^n(\boldsymbol{X}_c^n) - \boldsymbol{U}_c^n\right).$$

4. Update internal energy

$$m_c\left(\varepsilon_c^{n+\frac{1}{2}} - \varepsilon_c^n\right) - \frac{\Delta t}{2} \sum_{p \in \mathcal{P}(c)} \boldsymbol{F}_{cp}^n \cdot \boldsymbol{U}_p^n = 0.$$

5. Update vertex position

$$\boldsymbol{X}_p^{n+\frac{1}{2}} = \boldsymbol{X}_p^n + \frac{\Delta t}{2} \boldsymbol{U}_p^n.$$

6. Update volume and density

$$\rho_c^{n+\frac{1}{2}} = \frac{m_c}{V_c^{n+\frac{1}{2}}}, \qquad \rho_{cp}^{n+\frac{1}{2}} = \frac{m_{cp}}{V_{cp}^{n+\frac{1}{2}}}.$$

7. Compute predicted pressures

$$P_c^{n+\frac{1}{2}} = P\left(\rho_c^{n+\frac{1}{2}}, \varepsilon_c^{n+\frac{1}{2}}\right), \qquad P_{cp}^{n+\frac{1}{2}} = P\left(\rho_{cp}^{n+\frac{1}{2}}, \varepsilon_{cp}^{n+\frac{1}{2}}\right).$$

Corrector step

1. Piecewise monotonic linear reconstruction of the velocity field over the dual grid

$$\boldsymbol{U}_p^{n+\frac{1}{2}}(\boldsymbol{X}) = \boldsymbol{U}_p^n + \nabla \boldsymbol{U}_p^{\lim}(\boldsymbol{X} - \boldsymbol{X}_p^{n+\frac{1}{2}}).$$

2. Compute $\boldsymbol{U}_c^{n+1/2}$ with the high-order cell-centered Riemann solver

$$\boldsymbol{U}_c^{n+\frac{1}{2}} = \left(\mathsf{M}_c^{n+\frac{1}{2}}\right)^{-1} \sum_{p \in \mathcal{P}(c)} \left[-\left(L_{cp}\boldsymbol{N}_{cp}\right)^{n+\frac{1}{2}} P_{cp}^{n+\frac{1}{2}} + \mathsf{M}_{cp}^{n+\frac{1}{2}} \boldsymbol{U}_p^{n+\frac{1}{2}}(\boldsymbol{X}_c^{n+\frac{1}{2}}) \right].$$

3. Compute subcell forces

$$\boldsymbol{F}_{cp}^{n+\frac{1}{2}} = -\left(L_{cp}\boldsymbol{N}_{cp}\right)^{n+\frac{1}{2}} P_{cp}^{n+\frac{1}{2}} + \mathsf{M}_{cp}^{n+\frac{1}{2}} \left[\boldsymbol{U}_p^{n+\frac{1}{2}}(\boldsymbol{X}_c^{n+\frac{1}{2}}) - \boldsymbol{U}_c^{n+\frac{1}{2}}\right].$$

4. Update momentum

$$m_p\left(\boldsymbol{u}_p^{n+1}-\boldsymbol{u}_p^n\right)+\Delta t\sum_{c\in\mathcal{C}(p)}\boldsymbol{F}_{cp}^{n+\frac{1}{2}}=\boldsymbol{0}.$$

5. Update internal energy

$$m_c\left(\varepsilon_c^{n+1}-\varepsilon_c^n\right)-\Delta t\sum_{p\in\mathcal{P}(c)}\boldsymbol{F}_{cp}^{n+\frac{1}{2}}\cdot\boldsymbol{u}_p^{n+\frac{1}{2}}=0,$$

with $\boldsymbol{u}_p^{n+1/2}=(\boldsymbol{u}_p^{n+1}+\boldsymbol{u}_p^n)/2$.

6. Update vertex position

$$\boldsymbol{x}_p^{n+1}=\boldsymbol{x}_p^n+\Delta t\boldsymbol{u}_p^{n+\frac{1}{2}}.$$

7. Update volume and density

$$\rho_c^{n+1}=\frac{m_c}{V_c^{n+1}},\qquad \rho_{cp}^{n+1}=\frac{m_{cp}}{V_{cp}^{n+1}}.$$

8. Compute pressures

$$P_c^{n+1}=P\left(\rho_c^{n+1},\varepsilon_c^{n+1}\right),\qquad P_{cp}^{n+1}=P\left(\rho_{cp}^{n+1},\varepsilon_{cp}^{n+1}\right).$$

We point out that in the corrector step, internal energy has been discretized using the time centered nodal velocity $\boldsymbol{u}_p^{n+1/2}$. This choice is required to ensure total energy conservation up to machine precision.

7 Numerical results

The 2D Cartesian geometry is chosen for all test cases which are mono-material simulations. Only the ideal gas EOS is employed even though the framework accepts any type of EOS. We provide results of the following test cases: the Sod shock tube, the Cartesian Sedov problem, the Saltzman piston problem, the Noh problem and a Richtmyer-Meshkov instability. The high-order scheme is used for every test except the Sod shock tube for which a comparison between first and high-order is provided.

7.1 Sod shock tube

The Sod problem is a 1D Riemann shock tube with a relatively mild discontinuity. Its solution consists of a left moving rarefaction fan, a right moving contact discontinuity and a right moving shock wave. The domain is filled with an ideal gas at rest with $\gamma=1.4$. The density/pressure values on the left side of the discontinuity are 1.0/1.0, while those on the right side are 0.125/0.1. The discontinuity is initially located at 0.5.

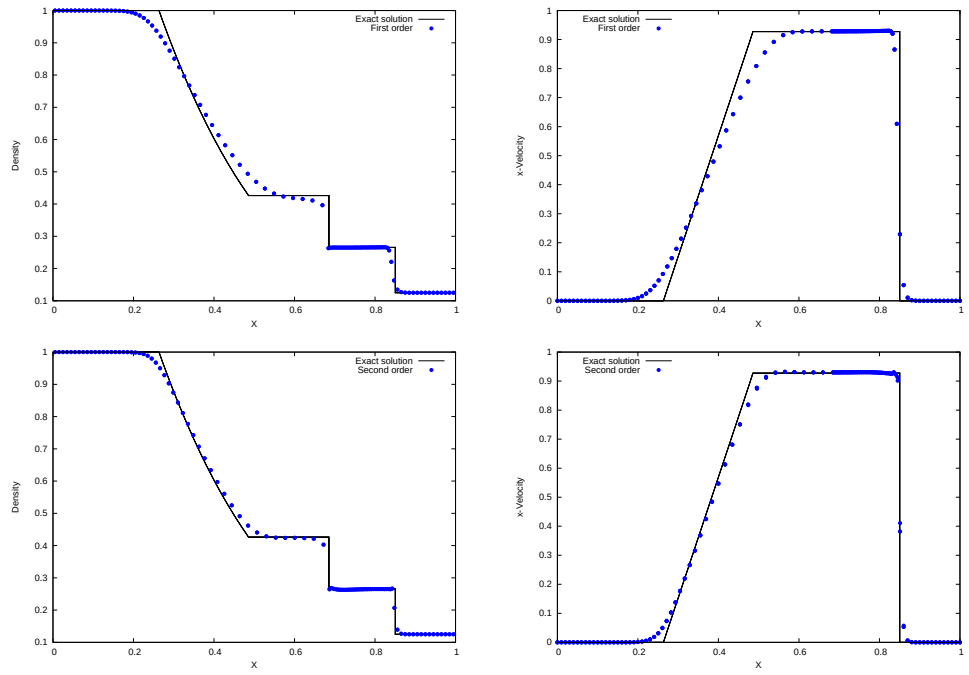

Figure 3: Sod problem at $t_{\text{final}}=0.2$ for 200 cells in x-direction. Top: first order scheme. Bottom: high order scheme. From left to right: Cell-centered density, nodal velocity in x-direction as a function of x.

We simulate this problem up to the final time $t_{\text{final}}=0.2$. In our numerical experiments, the computational domain is $\Omega=[0,1]\times[0,y_{\max}]$, where $y_{\max}$ is chosen so that the cells are initially squares. We are enforcing zero normal velocity at left and right of Ω and slip boundary at top and bottom. The run is made with $n_x=200$ computational cells in x direction and $n_y=10$ cells in y direction leading to $y_{\max}=0.2$.

In Fig. 3 is presented the first order (top) and high order extension (bottom). We display the cell density for all cells and the nodal velocity for all nodes *vs* the exact solution shown by solid line. The symmetry of the scheme is perfect and the quality of the high order results is close to the cell-centered Lagrangian scheme [26]. The first order scheme presents classical associated behavior-three-to-five cell shock spreading-whereas the shock wave is spread only on one or two cells for the second-order extension. In the compatible staggered Lagrangian scheme with classical artificial viscosity the shock is generally spread over three to five cells. Moreover the tail of the rarefaction does not suffer from the classical undershoot that can usually be seen on classical compatible staggered Lagrangian scheme.

7.2 Sedov blast wave problem

In this subsection we present the Sedov blast wave problem [31], which describes the evolution of a blast wave in a point-symmetric explosion. It is an example of a diverging

shock wave. We consider the cylindrically symmetric Sedov problem in Cartesian geometry. The total energy of the explosion is concentrated at the origin and has magnitude $E_{\text{total}}=0.244816$ similar to [22]. The material is an ideal gas with $\gamma=1.4$ and initially is at rest with an initial density equal to 1.0.

At final time $t_{\text{final}}=1.0$ the exact solution is a cylindrically symmetric diverging shock whose front is at radius $r=\sqrt{x^2+y^2}=1$ and has a density peak $\rho=6.0$. An exact solution is available as instance in [19]. In our numerical experiments E_{total} is concentrated in one cell located at the origin (that is, containing the vertex $(x,y)=(0,0)$). The specific internal energy of this cell, c, is defined as $\varepsilon_c=E_{\text{total}}/V_c$. Therefore the initial pressure for this cell is $p=(\gamma-1)\rho\varepsilon=0.4E_{\text{total}}/V_c$.

The high-order scheme is used. First we use a Cartesian grid of 30×30 cells on domain $\Omega=[0,1.2]\times[0,1.2]$ (see Fig. 4(a)). Next we use a polygonal grid (Voronoi tessellation) of a quarter of the disk of radius 1.2 (see Fig. 4(c)), this mesh has 775 cells being various polygons. In Fig. 4(a) are shown the mesh and the density colormap. The general geometric mesh quality is good. Moreover the symmetry of the shock wave is nicely preserved on both these meshes. Indeed the good symmetry preservation is shown on Fig. 4(b), (d) where the cell density as a function of cell radius is displayed for all cells in the domain together with the exact solution; not only the shock wave is very sharp but the cells are well distributed onto the exact curve.

7.3 Noh problem

In a quarter of the unit disk a gas ($\gamma=5/3$) is initiated with

$$\rho_0=1,\quad \varepsilon_0=10^{-6}\quad\text{and}\quad \mathbf{U}(x,y)=\Big(\frac{-x}{\sqrt{x^2+y^2}},\frac{-y}{\sqrt{x^2+y^2}}\Big).$$

A cylindrical shock wave is generated at the origin and further diverges. The final time is chosen at $t_{\text{final}}=0.6$. The exact solution at radius r and time t is given by the following relations, in which d identifies the geometry of the problem (1 for 1D Cartesian, 2 for 1D cylindrical, 3 for 1D spherical), ρ_0 is the uniform initial density, and u_0 is the uniform radial velocity ($u_0=\|\mathbf{U}\|=1$):

$$\{\rho,\varepsilon,u_r\}=\begin{cases}\Big\{\rho_0\Big(\dfrac{\gamma+1}{\gamma-1}\Big)^d,\dfrac{1}{2}(u_0)^2,0\Big\}, & \text{if } r<r_s,\\ \Big\{\rho_0\Big(1-\dfrac{u_0t}{r}\Big)^d,0,u_0\Big\}, & \text{if } r>r_s,\end{cases}\tag{7.1}$$

where the position of the shock r_s is given by

$$r_s=U_st,\ \text{ with the shock speed }\ U_s=\frac{1}{2}(\gamma-1)|u_0|.\tag{7.2}$$

The exact solution is given by ($r_s=0.2$, $U_s=1/3$)

$$\{\rho,\varepsilon,u_r\}=\begin{cases}\Big\{16,\dfrac{1}{2},0\Big\}, & \text{if } r<0.2,\\ \Big\{\Big(1+\dfrac{3}{5}\dfrac{1}{r}\Big),0,1\Big\}, & \text{if } r>0.2.\end{cases}\tag{7.3}$$

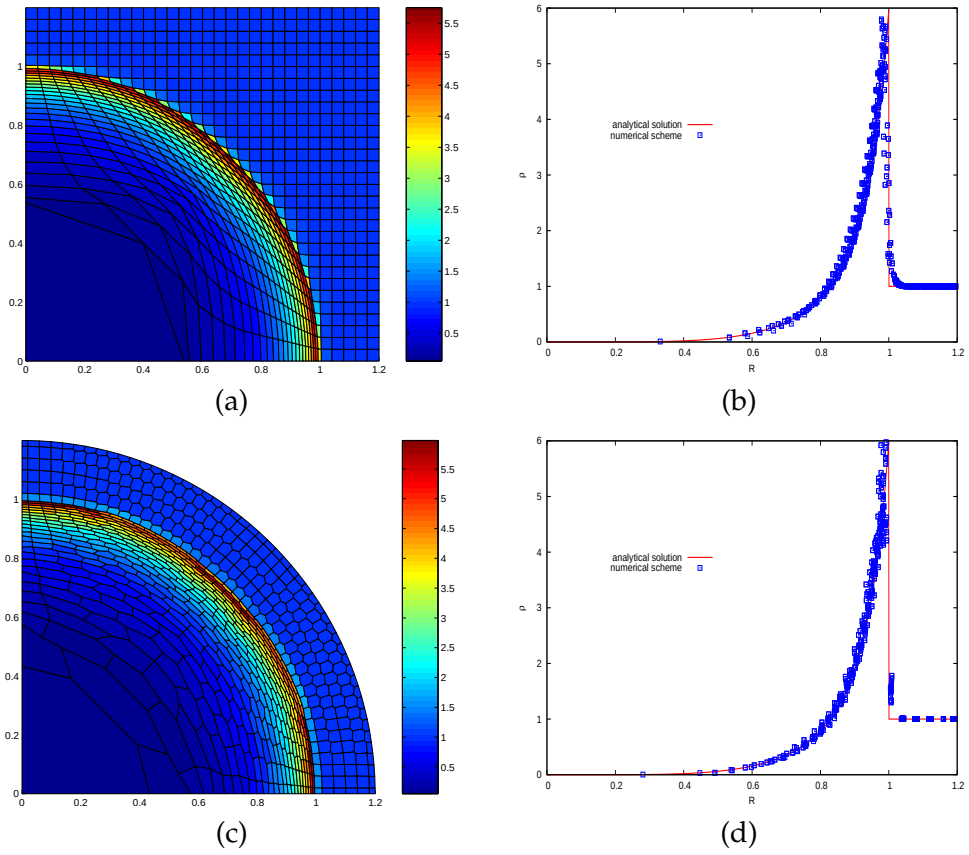

Figure 4: Sedov problem at $t_{\text{final}}=1$. (a) Density map and mesh on a 30×30 Cartesian grid. (b) Cell density as a function of cell center radius vs exact solution on a 30×30 Cartesian grid. (c) Density map and mesh on a polygonal grid. (d) Cell density as a function of cell center radius vs exact solution on a polygonal grid.

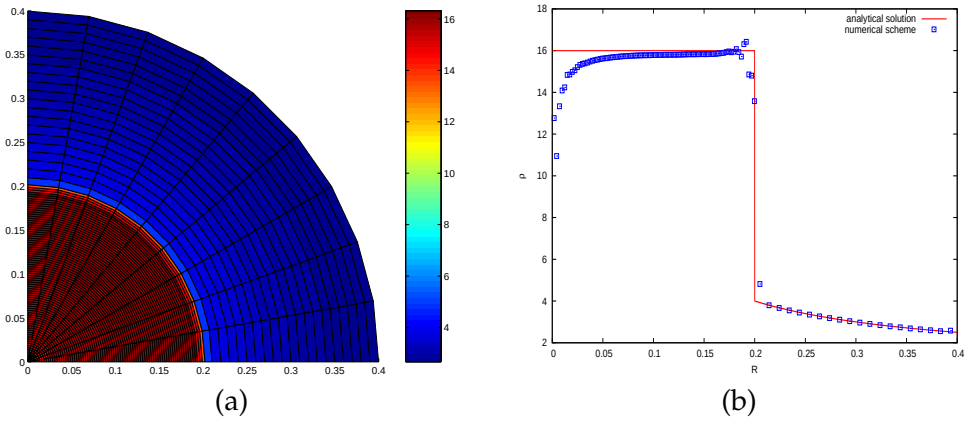

Figure 5: Noh problem at $t_{\text{final}}=0.6$ on a 100×9 polar grid. (a) Density map and mesh. (b) Cell density as a function of cell center radius vs exact solution.

This problem is simulated in its Cartesian version. First a polar mesh with 100 cells in radial direction and 9 cells in angular direction is considered. Fig. 5 shows the final mesh and density colormap on panel (a) and the cell density as a function of cell center radius compared to exact solution on panel (b). The symmetry of the shock wave and the mesh is almost perfect. Moreover the accuracy of the plateau is good and one observes a classical wall heating effect close to the origin. A slight overshoot can be noticed just after the shock wave which is, however, very sharp.

One classical issue of using polar mesh is the fact that to get a cell aspect ratio close to one on the external border of the disk we have to mesh the region close to the origin with triangles that have tremendously small internal angle. This leads not only to very big number of cells, but also to inaccuracy and sensitivity while discretizing equations on such long and a thin triangles, and last but not least, a small time step. A solution consists in using a non-conformal mesh as depicted in Fig. 6 panel (a); the mesh is made of quadrangles and every second angular line is stopped at a given radius ($r=0.3$ in the figure), leading to pentagonal cells. Such lines and associated cells are elsewhere referred as to termination lines [21] or dendritic cells. The extra nodes that are created on these pentagons by the termination lines are usually enslaved to their edge. A special treatment is set-up for these pentagonal cells [21] in classical compatible Lagrangian hydrodynamics scheme. This treatment is based on distribution of masses and forces on surrounding zones. In our approach, as for the cell-centered Lagrangian scheme [26], no special treatment is needed. The Riemann solver is naturally producing the correct point velocity (see Fig. 6(b)) contrary to the classical approach with no special treatment (see Fig. 9(a) on page 11 of [21]). Although some mesh imprint can be seen, the cell density as a function of cell center radius in Fig. 6(c) is still very well reproduced.

7.4 Saltzman piston

The domain $\Omega=[0,1]\times[0,0.1]$ is filled with a gas ($\gamma=5/3$) at rest $\rho=1$, $\varepsilon=10^{-6}$. The right boundary is a perfect wall, the left boundary is a right-moving piston with velocity $\boldsymbol{U}=(1,0)^t$. This piston sends a straight shock wave into the rectangular domain. This shock wave ultimately bounces onto the fixed right wall and onto the piston back and forth. At time $t=1.0$ the piston reaches the right wall.

An exact solution is defined by the value of the plateaus behind the shock. The analytical solution is characterized by a post-shock density plateau of 4 and a shock velocity of $4/3$ before the time $t=0.75$. This problem usually tests the robustness of Lagrangian numerical methods by using the Saltzman mesh defined by $n_x=100$ cells in x-direction and $n_y=10$ in y-direction and a deformation in x-direction as

$$x_{\text{deformed}}=x+(0.1-y)\sin(\pi x),$$

as can be seen in Fig. 7. In Fig. 8 is presented the mesh and the density colormap at time $t_{\text{final}}=0.6$. Unfortunately, our approach is not able to perform up to time $t>0.925$ as the top left corner cells are pinched and become tangled soon after this time. This

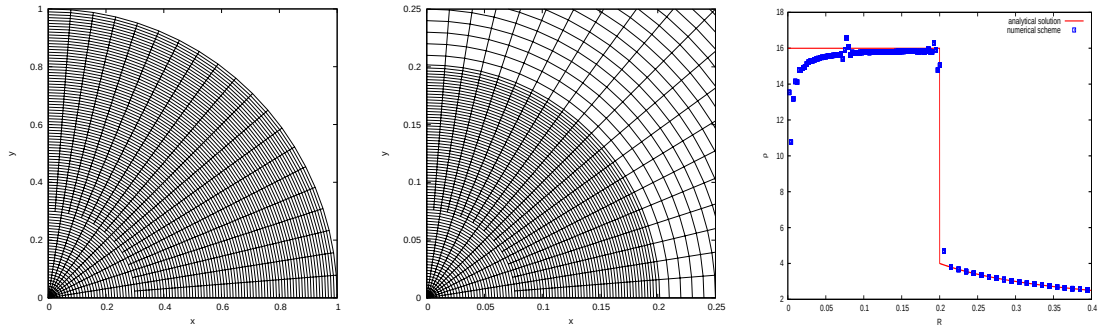

(a) (b) (c)

Figure 6: Noh problem at $t_{\text{final}}=0.6$ on a non-conformal grid. (a) Initial mesh. (b) Zoom on the final mesh. (c) Cell density as a function of cell center radius vs exact solution.

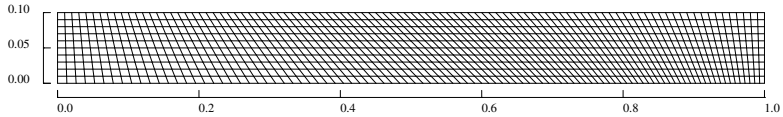

Figure 7: Saltzman piston. Initial skewed mesh.

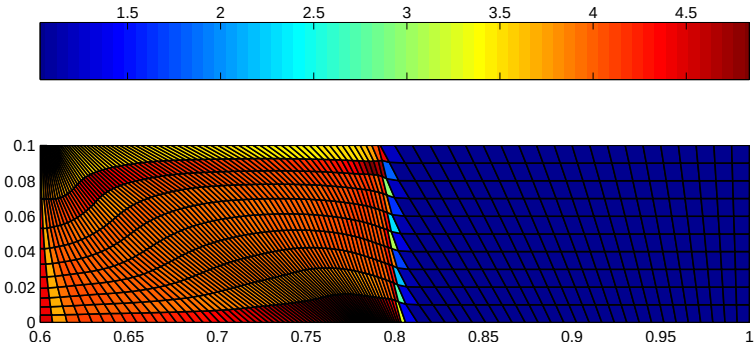

Figure 8: Saltzman piston at time $t_{\text{final}}=0.6$. Final mesh and density colormap.

quite disappointing result asks for more investigation on robustness issue and also on boundary condition treatment using staggered discretization.

7.5 Linear phase of Richtmyer-Meshkov instability

This test case is devoted to the study of the linear phase of the Richtmyer-Meshkov instability [30] for a piston-driven flow. This hydrodynamic instability occurs when a shock wave hits a perturbed interface separating two different fluids. For sufficiently small perturbations, analytical solutions can be derived using linear perturbation theory [36]. In this framework, the theory shows that the amplitude of the perturbation grows linearly as a function of time. We first study the unperturbed fluid configuration in the RMI prob-

lem, which is a collision of a shock wave with a flat contact discontinuity. Such collision produces a transmitted shock wave and a reflected wave that can be either a shock or a rarefaction. This shock-contact interaction defines a one-dimensional Riemann problem, which can be solved analytically.

In what follows, we will employ the configuration displayed in Fig. 9. The interface is located at $x=0$ and the computational domain corresponding to the shock tube is defined by $(x,y)\in[-5,4.2]\times[0,0.5]$, since the $y=0$ line is a symmetry axis for this problem. For the initial and boundary conditions described in Fig. 9, the incident piston-driven shock hits the interface at time $t=3.015$. This interaction leads to transmitted and reflected shock waves, which also later interact with the piston and the right boundary wall. The time history of the shock-contact interaction is displayed in Fig. 10(a) using a classical $(t-x)$ diagram. We run a computation for the unperturbed configuration with our high-order scheme using 460 equally spaced cells in the x-direction and one cell in the y-direction. The density as function of x-coordinate is plotted in Fig. 10(b) together with analytical solution at time $t=5$. We point out the very good agreement between numerical and analytical solutions. Moreover, we note that transmitted and reflected shocks are sharply resolved. In order to study the perturbed configuration, we initialize a cosinusoidal perturbation of the interface with a small amplitude a_0. Thus, the equation of the interface is written

$$x(y)=a_0\cos\Big(\frac{2\pi}{\lambda}y\Big),\quad \text{for } y\in\Big[-\frac{\lambda}{2},\frac{\lambda}{2}\Big], \tag{7.4}$$

where λ is the wavelength of the perturbation. The shape of the perturbed interface is displayed in Fig. 9. For a small enough initial amplitude, linear theory predicts that the perturbation amplitude, $a(t)$, grows linearly as a function of time, after the shock has interacted with the interface. Using direct two-dimensional simulation of the perturbed configuration, we shall recover this important result and compare the numerical perturbation amplitude with the one coming from the linear theory. The numerical simulations are made by meshing the computational domain, $(x,y)\in[-5,4.2]\times[0,0.5]$, with 460×25 equally spaced cells. Hence, we have set $\lambda=1$ and meshed only a half wavelength due to the symmetry of the problem w.r.t. x-axis. We set $a_0=10^{-4}$ and performed a computation utilizing our high-order scheme. The perturbed interface is prescribed by moving the vertices initially located on the line $x=0$ onto the curve defined by Eq. (7.4). The perturbation amplitude, $a(t)$, is computed using the following formula

$$a(t)=\frac{X_{\text{pert}}(t)-X_{\text{unpert}}(t)}{a_0}, \tag{7.5}$$

where $X_{\text{pert}}(t)$ (resp. $X_{\text{unpert}}(t)$) is the abscissa of a point located on the perturbed (resp. unperturbed) interface. Using this formula for the previous computations, we compute the corresponding perturbation amplitude and compare it to the reference one coming from the linear theory [36]. We have plotted in Fig. 11 the numerical perturbation amplitude as a function of time compared to the one coming from the linear theory. We

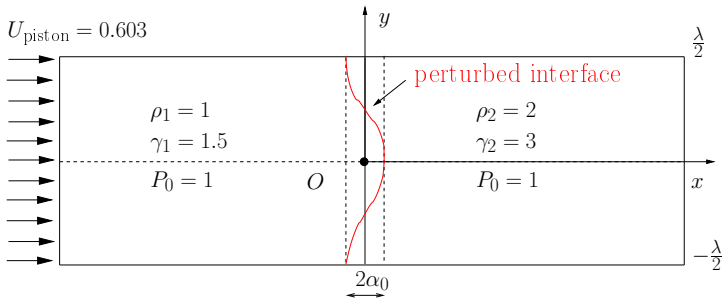

Figure 9: Richtmyer-Meshkov instability initialization.

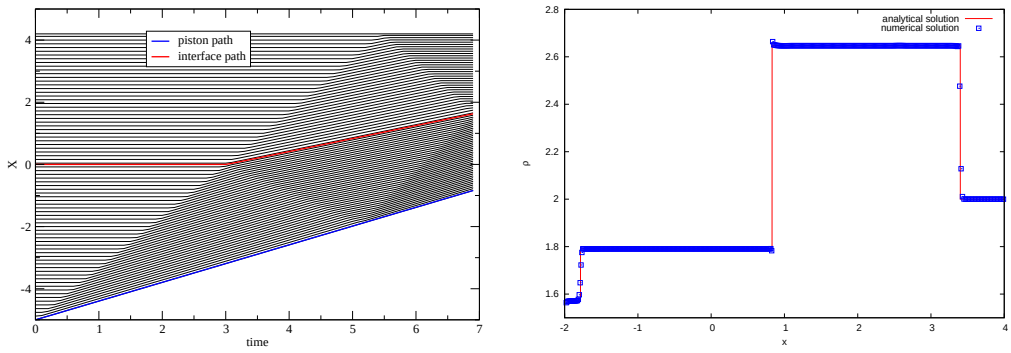

(a) (b)

Figure 10: Richtmyer-Meshkov instability. (a) Time-X diagram where piston and interface paths are displayed. (b) Density as a function of X coordinate *vs* analytical solution at $t=5$.

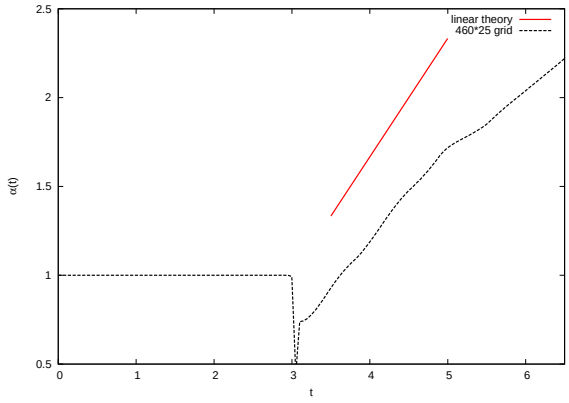

Figure 11: Shock-contact interaction problem. Numerical perturbation amplitude as a function of time *vs* linear theory.

remark that the high-order computation recovers quite well the linear theory. These results show the ability of our high-order Lagrangian scheme to simulate very accurately complex phenomena such as hydrodynamic instabilities.

8 Conclusions

This work suggests a general formalism to derive staggered discretizations for Lagrangian hydrodynamics on general unstructured meshes in two dimensions. The framework uses fundamental objects of compatible discretizations like Lagrangian subcell mass and subcell forces. Artificial viscosity form is formulated invoking Galilean invariance and thermodynamic consistency. The satisfaction of entropy inequality is ensured by using a subcell-based symmetric positive definite tensor, a particular example of which is given in this work. An extension to high order in space and time is demonstrated, including a vector limitation procedure which is frame independent and thus preserves desirable properties like rotational symmetry. Performance of the new method is demonstrated on a set of classical and demanding numerical tests, using various structured and unstructured computational meshes.

An important potential link between staggered and cell-centered Lagrangian schemes is the viscous part of subcell force. While some of the existing artificial viscosity implementations can be easily reformulated by means of the proposed symmetric positive definite tensor, others still seem to resist this simple interpretation. From this viewpoint there remains enough space for deeper investigation with the prospect of finding important similarities and differences between the Godunov-based and Lagrange-based methods.

Another promising idea to be explored is the use of a generalized Riemann problem [5] for simultaneous discretization in space and time, which would replace predictor-corrector temporal integration by a more elegant one-step scheme.

Last but not least, the plan is to extend all pieces of the existing machinery to two-dimensional axisymmetric [25] and further to three-dimensional geometry and thus open it for new practical applications.

Acknowledgments

The authors would like to thank Milan Kucha̋řík, Richard Liska, Misha Shashkov and Burt Wendroff for fruitful discussions. The last author has been partly supported by the Czech Ministry of Education grants MSM 6840770022, MSM 6840770010, LC528 and the Czech Science Foundation grant P205/10/0814.

Appendix: 1D staggered Lagrangian scheme based on cell-centered Riemann solver

In this appendix we detail the 1D version of the numerical scheme proposed in this paper. In order to be complete we fully describe its derivation. The governing equations are

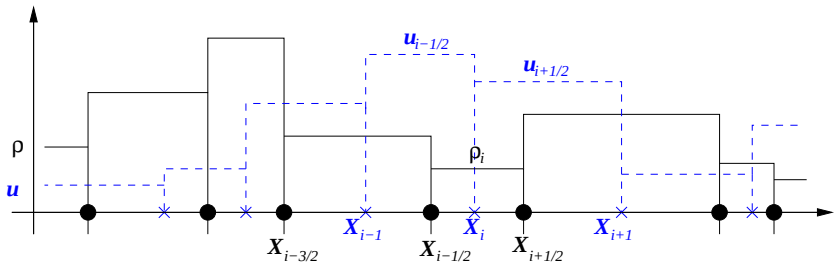

Figure 12: Notation for the 1D scheme description.

written in 1D as

$$\rho\frac{d}{dt}\left(\frac{1}{\rho}\right)-\frac{\partial}{\partial X}u=0,\qquad \rho\frac{d}{dt}u+\frac{\partial}{\partial X}P=0,\qquad \rho\frac{d}{dt}E+\frac{\partial}{\partial X}(Pu)=0. \tag{A.1}$$

Physical variables are expressed as functions of $X(t)$, which is the coordinate of a fluid particle at time t whose initial position is denoted by x. The trajectory equation then writes

$$\frac{d}{dt}X=u(X(t),t),\qquad X(0)=x. \tag{A.2}$$

A cell is labeled with an integer index as I_i and is the segment $I_i(t)=[X_{i-1/2}(t);X_{i+1/2}(t)]$ constituted of two consecutive points labeled with half-integers, see Fig. 12. $I=\bigcup_i I_i$ is a partition of the 1D computational domain. We denote $V_i(t)=X_{i+1/2}(t)-X_{i-1/2}(t)$ the volume of cell I_i. The displacement of the vertex $X_{i+1/2}(t)$ is given by the semi-discrete trajectory equation

$$\frac{d}{dt}X_{i+\frac{1}{2}}=u_{i+\frac{1}{2}},\qquad X_{i+\frac{1}{2}}(0)=x_{i+\frac{1}{2}}, \tag{A.3}$$

where $u_{i+1/2}=u(X_{i+1/2}(t),t)$ is the trajectory of the vertex, namely the fluid velocity at point $X_{i+1/2}$. Since cell I_i moves with the fluid velocity it may deform but can neither gain nor lose mass, thus the mass of cell I_i writes

$$m_i(t)=\int_{I_i(t)}\rho(X(t),t)\,\mathrm{d}X=\int_{I_i(0)}\rho(x,0)\,\mathrm{d}x=m_i(0), \tag{A.4}$$

where $I_i(0)=[x_{i-1/2},x_{i+1/2}]$ is the initial cell and $\rho(x,0)$ the initial density. Let

$$X_i(t)=\frac{1}{2}\left(X_{i-\frac{1}{2}}(t)+X_{i+\frac{1}{2}}(t)\right)$$

be the center of cell I_i. The median mesh is defined by the introduction of the dual cell $I_{i+1/2}(t)=[X_i(t),X_{i+1}(t)]$. Knowing that the cell center is computed in a Lagrangian manner we deduce that the mass of the dual cell, $m_{i+1/2}$, is constant and writes $m_{i+1/2}=(m_i+m_{i+1})/2$.

Volume conservation equation. Let $\rho_i(t)$ be the cell-averaged density

$$\rho_i(t)=\frac{1}{V_i(t)}\int_{I_i(t)}\rho(X(t),t)\mathrm{d}X. \tag{A.5}$$

It can also be written $\rho_i(t)=m_i/V_i(t)$ and therefore

$$m_i\frac{d}{dt}\Big(\frac{1}{\rho_i}\Big)=\frac{d}{dt}V_i=u_{i+\frac{1}{2}}-u_{i-\frac{1}{2}}, \tag{A.6}$$

which is the semi-discrete version of the volume conservation equation (A.1).

Momentum conservation equation. The semi-discrete momentum equation over the dual cell writes

$$m_{i+\frac{1}{2}}\frac{d}{dt}u_{i+\frac{1}{2}}+\big(P^*_{i+1}-P^*_i\big)=0, \tag{A.7}$$

where $P^*_i=P(X_i(t),t)$ represents the pressure at zone center X_i that remains to be determined.

Total energy conservation. Without taking into account boundary terms we introduce the total kinetic energy at time $t>0$ as

$$\mathcal{K}=\sum_{i+\frac{1}{2}}\frac{1}{2}m_{i+\frac{1}{2}}u^2_{i+\frac{1}{2}},$$

where the sum is performed over the dual cells $I_{i+1/2}$. We also introduce the total internal energy at t as $\mathcal{E}=\sum_i m_i\varepsilon_i$, where the sum is taken over the primal cells I_i and ε_i denotes the cell-averaged internal energy. Conservation of total energy writes

$$\frac{d}{dt}\mathcal{K}+\frac{d}{dt}\mathcal{E}=0. \tag{A.8}$$

Recalling that masses are Lagrangian objects, the previous equation rewrites

$$\sum_{i+\frac{1}{2}}\frac{1}{2}m_{i+\frac{1}{2}}u_{i+\frac{1}{2}}\frac{d}{dt}u_{i+\frac{1}{2}}=-\sum_i m_i\frac{d}{dt}\varepsilon_i. \tag{A.9}$$

Substituting the semi-discrete momentum equation previously derived we get

$$\sum_{i+\frac{1}{2}}u_{i+\frac{1}{2}}(P^*_{i+1}-P^*_i)=\sum_i m_i\frac{d}{dt}\varepsilon_i, \tag{A.10}$$

which yields after shifting the index of the first sum

$$\sum_i P^*_i\big(u_{i+\frac{1}{2}}-u_{i-\frac{1}{2}}\big)=\sum_i m_i\frac{d}{dt}\varepsilon_i. \tag{A.11}$$

Without taking into account the boundary terms, the total energy conservation writes

$$\sum_i m_i \frac{d}{dt}\varepsilon_i + P_i^* \left(u_{i+\frac{1}{2}} - u_{i-\frac{1}{2}}\right) = 0. \tag{A.12}$$

A sufficient condition to ensure total energy conservation is obtained by writing the following evolution equation for the internal energy within cell I_i

$$m_i \frac{d}{dt}\varepsilon_i + P_i^* \left(u_{i+\frac{1}{2}} - u_{i-\frac{1}{2}}\right) = 0. \tag{A.13}$$

The only unknown to determine is the pressure P_i^*. Let us note that using the volume conservation equation this last equation can be recast into the form

$$m_i \frac{d}{dt}\varepsilon_i + m_i P_i^* \frac{d}{dt}\left(\frac{1}{\rho_i}\right) = 0, \tag{A.14}$$

which, recalling the Gibbs formula $TdS = d\varepsilon + Pd(\frac{1}{\rho})$, rewrites

$$m_i T_i \frac{d}{dt} S_i = -m_i (P_i^* - P_i) \frac{d}{dt}\left(\frac{1}{\rho_i}\right), \tag{A.15}$$

where S_i and T_i are the specific entropy and temperature in cell I_i. The right-hand side of this equation is nothing but the time rate of change of specific entropy dissipation. According to the second law of thermodynamics $T_i \frac{d}{dt} S_i \geq 0$, thus we should have

$$(P_i^* - P_i) \frac{d}{dt}\left(\frac{1}{\rho_i}\right) \leq 0.$$

Consequently for smooth flows, characterized by reversible thermodynamical process, such as rarefaction wave or isentropic compression, we should have $P_i^* = P_i$ since $\frac{d}{dt}(\frac{1}{\rho_i}) < 0$. The difference $P_i^* - P_i$ is the artificial viscosity first introduced by von Neumann and Richtmyer [33]. Let us now describe how to compute this term by solving a staggered Riemann problem. First the interfacial pressure P_i^* is computed at each cell center X_i by solving the Riemann problem characterized by the left state $(\rho_i, u_{i-1/2}, P_i)$ and the right one $(\rho_i, u_{i+1/2}, P_i)$. Note that only the velocity is discontinuous with a jump

$$\Delta u = u_{i+\frac{1}{2}} - u_{i-\frac{1}{2}}.$$

In order to simplify the notation let us denote with subscript L the left state (ρ, u_L, P). Accordingly the right state is (ρ, u_R, P) with subscript R and the jump in velocity is $\Delta u = u_R - u_L$. We note that the equation of state is the same both sides of the interface. The solution of the Riemann problem is a two-shock solution in the case that $\Delta u < 0$ (see Fig. 13 top-right panel) and a two-rarefaction solution if $\Delta u > 0$ (see Fig. 13 bottom-right

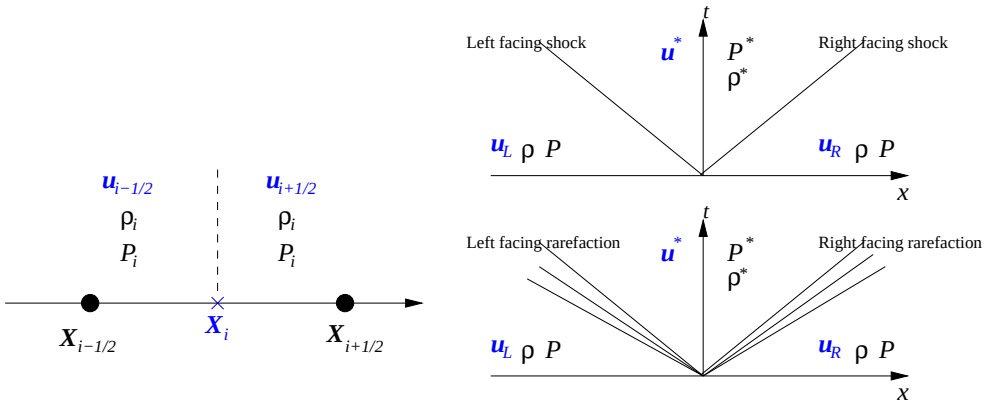

Figure 13: Left: States for the Riemann problem at cell center. Top-right: Two-shock Riemann solution. Bottom-right: Two-rarefaction Riemann solution.

panel). The solution is denoted (ρ^*,u^*,P^*). Since thermodynamical variables are continuous across the interface, there is no contact discontinuity.

Two-shock case. The Rankine-Hugoniot relations allow to compute the post-shock pressure and velocity. They write for the right-facing shock

$$M\left(\frac{1}{\rho^*}-\frac{1}{\rho}\right)=-(u^*-u_R), \tag{A.16a}$$

$$M(u^*-u_R)=P^*-P, \tag{A.16b}$$

$$\varepsilon^*-\varepsilon+\frac{P^*+P}{2}\left(\frac{1}{\rho^*}-\frac{1}{\rho}\right)=0, \tag{A.16c}$$

where $M>0$ denotes the mass swept by the wave per unit time. For the left-facing shock we only write

$$M\left(\frac{1}{\rho^*}-\frac{1}{\rho}\right)=-(u^*-u_L), \tag{A.17a}$$

$$M(u^*-u_L)=-(P^*-P), \tag{A.17b}$$

recalling that the third equation is exactly the same as (A.16c) since it is independent on the direction of propagation. Adding (A.16b) and (A.17b) yields $u^*=(u_R+u_L)/2$, hence using (A.16b) and the definition of Δu we get

$$P^*=P-\frac{1}{2}M\Delta u. \tag{A.18}$$

Using cell notation we deduce

$$P_i^*=P_i-\frac{1}{2}M\left(u_{i+\frac{1}{2}}-u_{i-\frac{1}{2}}\right), \tag{A.19}$$

thus the internal energy equation reads

$$m_i \frac{d}{dt}\varepsilon_i + P_i\left(u_{i+\frac{1}{2}} - u_{i-\frac{1}{2}}\right) = \frac{1}{2}M_i\left(u_{i+\frac{1}{2}} - u_{i-\frac{1}{2}}\right)^2. \tag{A.20}$$

This discretization is compatible with the second principle of thermodynamics.

The swept mass flux can be expressed as function of the physical variables by combining (A.16a) and (A.16b)

$$M^2 = -(P^* - P)\left(\frac{1}{\rho^*} - \frac{1}{\rho}\right)^{-1}. \tag{A.21}$$

In the limit of the weak shock wave $P^* \to P$ and $\rho^* \to \rho$ and one can show that $M \to \rho c$ where $c^2 = (\frac{\partial P}{\partial \rho})_s$ is the isentropic sound speed. In the general case for a γ gas law one can compute the analytical solution of the Riemann problem. Knowing that $P = (\gamma - 1)\rho\varepsilon$ and using (A.16c) one gets

$$\frac{1}{\rho^*} = \frac{1}{\rho}\frac{(\gamma+1)P + (\gamma-1)P^*}{(\gamma+1)P^* + (\gamma-1)P}. \tag{A.22}$$

After substitution in the equation for M^2 we obtain

$$M^2 = \rho\left(\frac{\gamma+1}{2}P^* + \frac{\gamma-1}{2}P\right), \tag{A.23}$$

thus using (A.16b) we show that P^* satisfies a quadratic equation whose physical solution is

$$P^* = P + \rho\left(\frac{\gamma+1}{4}\frac{\Delta u}{2} - \sqrt{\left(\frac{\gamma+1}{4}\right)^2\left(\frac{\Delta u}{2}\right)^2 + c^2}\right)\frac{\Delta u}{2}. \tag{A.24}$$

This last equation allows to write

$$M = \rho\left(-\frac{\gamma+1}{4}\frac{\Delta u}{2} + \sqrt{\left(\frac{\gamma+1}{4}\right)^2\left(\frac{\Delta u}{2}\right)^2 + c^2}\right). \tag{A.25}$$

Let us remark that this last equation recovers the Kuropatenko artificial viscosity [20] up to a factor one half in front of the velocity jump. Kuropatenko has in fact derived his formula computing the pressure jump produced by only one shock wave created by a velocity jump Δu. Here we are considering the solution of the Riemann problem corresponding to an initial velocity jump Δu. This initial discontinuity breaks up into two shock waves, each being characterized by a velocity jump of $\Delta u/2$. The same conclusion has been given by Luttwak and Falcovitz [24].

In the case of real material we propose the following ansatz for the swept mass flux

$$M = \rho\left(-c_0\frac{\Delta u}{2} + c_1 c\right), \tag{A.26}$$

where c_0 and c_1 are constants depending on material properties. This amounts to pretend that the velocity of the shock wave is an affine function of the fluid velocity. This assumption is satisfied for many materials as it has been noticed by Dukowicz [16]. Returning to cell notation we finally get

$$P_i^* = P_i - \frac{1}{2} M_i \left(u_{i+\frac{1}{2}} - u_{i-\frac{1}{2}} \right), \tag{A.27}$$

where

$$M_i = \rho_i \left(-c_0 \frac{1}{2} \left(u_{i+\frac{1}{2}} - u_{i-\frac{1}{2}} \right) + c_1 c_i \right). \tag{A.28}$$

Let us remark that this form of swept mass flux is the one used in (5.4) in 2D. Moreover, in 1D, the subcell matrix (5.7) is a 1×1 matrix that indeed coincides with the swept mass flux, hence the notation M_i in the equation above. Finally this procedure can be viewed as the solution of the Riemann problem using an approximate solver.

Two-rarefaction case. In the case $\Delta u \geq 0$ we simply can set $P_i^* = P_i$ in order to satisfy entropy conservation. It consists in canceling the entropy production in the case of rarefaction wave. This is the usual way of proceeding when dealing with classical artificial viscosity. However it is possible also to solve the Riemann problem in this case. Since $\Delta u \geq 0$, the initial discontinuity breaks up into two rarefaction waves (see Fig. 13 bottom-right panel). The Riemann problem is solved using Riemann invariants:

- for the right-facing wave $u^* - u_R = \int_\rho^{\rho^*} \frac{d\overline{P}}{\rho(\overline{P}) c(\overline{P})}$,
- for the left-facing wave $u^* - u_L = -\int_\rho^{\rho^*} \frac{d\overline{P}}{\rho(\overline{P}) c(\overline{P})}$,

and by adding these last equations we get $u^* = (u_R + u_L)/2$. In the case of a γ gas law one can integrate the Riemann invariants to get

$$P^* = P \left(1 - \frac{\gamma - 1}{2} \frac{\Delta u}{2c} \right)^{\frac{2\gamma}{\gamma - 1}}, \tag{A.29}$$

that is valid for

$$\frac{\Delta u}{2} \leq \frac{2}{\gamma - 1} c.$$

We can rewrite the last equation as

$$P^* = P + P \left[\left(1 - \frac{\gamma - 1}{2} \frac{\Delta u}{2c} \right)^{\frac{2\gamma}{\gamma - 1}} - 1 \right] = P - \frac{1}{2} M \Delta u, \tag{A.30}$$

where

$$M = P \left[- \left(1 - \frac{\gamma - 1}{2} \frac{\Delta u}{2c} \right)^{\frac{2\gamma}{\gamma - 1}} + 1 \right] \left(\frac{1}{2} \Delta u \right)^{-1} > 0. \tag{A.31}$$

In the limit of weak shock wave $\Delta u \to 0$ and thus $M \to \rho c$. For real materials one can derive an approximate solution using the following quadrature for the integrals for the Riemann invariants

$$\int_{\rho}^{\rho^*} \frac{d\overline{P}}{\rho(\overline{P})c(\overline{P})} = \frac{P^*-P}{\rho c}, \tag{A.32}$$

hence u^* and P^* are solution of the 2×2 linear system

$$\rho c(u^*-u_R) = P^*-P, \qquad \rho c(u^*-u_L) = -(P^*-P), \tag{A.33}$$

in particular $u^* = (u_L+u_R)/2$ and $P^* = P-\rho c\frac{\Delta u}{2}$. This corresponds to the acoustic approximation.

Time discretization. A two-step Runge-Kutta discretization is used. Knowing all physical quantities at time t^n, we advance them up to time $t^{n+1} = t^n + \Delta t$.

- **Predictor step.** One computes

$$P_i^{*,n} = P_i^n - \frac{1}{2}M_i^n \Delta u_i^n,$$

and solves the internal energy equation

$$m_i\left(\varepsilon_i^{n+\frac{1}{2}} - \varepsilon_i^n\right) + \frac{\Delta t}{2}P_i^{*,n}\left(u_{i+\frac{1}{2}}^n - u_{i-\frac{1}{2}}^n\right) = 0. \tag{A.34}$$

Then the mesh nodes are displaced:

$$X_{i+\frac{1}{2}}^{n+\frac{1}{2}} = X_{i+\frac{1}{2}}^n + \frac{\Delta t}{2}u_{i+\frac{1}{2}}^n.$$

The density is then computed:

$$\rho_{i+\frac{1}{2}}^{n+\frac{1}{2}} = m_i\left(V_i^{n+\frac{1}{2}}\right)^{-1},$$

where

$$V_i^{n+\frac{1}{2}} = X_{i+\frac{1}{2}}^{n+\frac{1}{2}} - X_{i-\frac{1}{2}}^{n+\frac{1}{2}}.$$

Finally the predicted pressure is computed

$$P_i^{n+\frac{1}{2}} = P(\rho_i^{n+\frac{1}{2}}, \varepsilon_i^{n+\frac{1}{2}}).$$

- **Corrector step.** One computes

$$P_i^{*,n+\frac{1}{2}} = P_i^{n+\frac{1}{2}} - \frac{1}{2}M_i^{n+\frac{1}{2}}\Delta u_i^n,$$

and solves momentum equation

$$m_{i+\frac{1}{2}}\left(u_{i+\frac{1}{2}}^{n+1} - u_{i+\frac{1}{2}}^n\right) + \Delta t\left(P_{i+1}^{*,n+\frac{1}{2}} - P_i^{*,n+\frac{1}{2}}\right) = 0, \tag{A.35}$$

and computes

$$u_{i+\frac{1}{2}}^{n+\frac{1}{2}} = \frac{1}{2}\left(u_{i+\frac{1}{2}}^{n+1} - u_{i+\frac{1}{2}}^{n}\right).$$

The internal energy is solved

$$m_i\left(\varepsilon_i^{n+1} - \varepsilon_i^n\right) + \Delta t P_i^{*,n+\frac{1}{2}}\left(u_{i+\frac{1}{2}}^{n+\frac{1}{2}} - u_{i-\frac{1}{2}}^{n+\frac{1}{2}}\right) = 0. \tag{A.36}$$

Then the mesh nodes are displaced:

$$X_{i+\frac{1}{2}}^{n+1} = X_{i+\frac{1}{2}}^{n} + \Delta t u_{i+\frac{1}{2}}^{n+\frac{1}{2}}.$$

The density is then computed:

$$\rho_{i+\frac{1}{2}}^{n+1} = m_i\left(V_i^{n+1}\right)^{-1},$$

where

$$V_i^{n+1} = X_{i+\frac{1}{2}}^{n+1} - X_{i-\frac{1}{2}}^{n+1}.$$

High-order extension of this scheme is obtained using a piecewise linear conservative reconstruction of the velocity on each dual cell.

$$\forall X \in [X_i, X_{i+1}], \quad u_{i+\frac{1}{2}}(X) = u_{i+\frac{1}{2}} + \delta u_{i+\frac{1}{2}}\left(X - \widetilde{X}_{i+\frac{1}{2}}\right), \tag{A.37}$$

where $\widetilde{X}_{i+1/2} = (X_i + X_{i+1})/2$ and we note that generally $\widetilde{X}_{i+1/2} \neq X_{i+1/2}$ since the mesh may be non-uniform. The reconstruction is conservative in the sense that

$$\frac{1}{X_{i+1} - X_i}\int_{X_i}^{X_{i+1}} u_{i+\frac{1}{2}}(X)\,\mathrm{d}X = u_{i+\frac{1}{2}}. \tag{A.38}$$

As instance a least squares approach is utilized to compute the slope $\delta u_{i+1/2}$. Monotonicity is ensured by the use of any classical slope limiter. High-order reconstructed velocities

$$u_L = u_{i-\frac{1}{2}}(X_i) = u_{i-\frac{1}{2}} + \delta u_{i-\frac{1}{2}}\left(X_i - \widetilde{X}_{i-\frac{1}{2}}\right)$$

and

$$u_R = u_{i+\frac{1}{2}}(X_i) = u_{i+\frac{1}{2}} + \delta u_{i+\frac{1}{2}}\left(X_i - \widetilde{X}_{i+\frac{1}{2}}\right)$$

are further used in the Riemann solver as left and right states.

References

[1] F. L. Addessio, D. E. Carroll, J. K. Dukowicz, F. H. Harlow, J. N. Johnson, B. A. Kashiwa, M. E. Maltrud and H. M. Ruppel, CAVEAT: a computer code for fluid dynamics problems with large distortion and internal slip, Technical Report LA-10613-MS, Los Alamos National Laboratory, 1986.

[2] T. J. Barth, Numerical methods for gasdynamic systems on unstructured meshes, in D. Kroner, M. Ohlberger and C. Rohde, editors, An Introduction to Recent Developments in Theory and Numerics for Conservation Laws, Proceedings of the International School on Theory and Numerics for Conservation Laws, pages 195–284, Berlin, 1997; Lecture Notes in Computational Science and Engineering, Springer.
[3] T. J. Barth and D. C. Jespersen, The design and application of upwind schemes on unstructured meshes, in AIAA paper 89-0366, 27th Aerospace Sciences Meeting, Reno, Nevada, 1989.
[4] A. L. Bauer, D. E. Burton, E. J. Caramana, R. Loubère, M. J. Shashkov and P. P. Whalen, The internal consistency, stability, and accuracy of the discrete, compatible formulation of Lagrangian hydrodynamics, J. Comput. Phys., 218(2) (2006), 572–593.
[5] M. Ben-Artzi and J. Falcovitz, Generalized Riemann problems in computational fluid dynamics, Cambridge Monographs on Applied and Computational Mathematics, Cambridge University Press, Cambridge, UK, 2003.
[6] A. Burbeau-Augoula, A node-centered artificial viscosity method for two-dimensional Lagrangian hydrodynamics calculations on a staggered grid, Commun. Comput. Phys., 8(4) (2010), 877–900.
[7] D. E. Burton, Exact conservation of energy and momentum in staggered-grid hydrodynamics with arbitrary connectivity, Advances in the Free Lagrange Method, Springer-Verlag, New-York, 1990.
[8] J. C. Campbell and M. J. Shashkov, A tensor artificial viscosity using a mimetic finite difference algorithm, J. Comput. Phys., 172(4) (2001), 739–765.
[9] J. C. Campbell and M. J. Shashkov, A compatible Lagrangian hydrodynamics algorithm for unstructured grids, Seluk J. Appl. Math., 4(2) (2003), 53–70.
[10] E. J. Caramana, D. E. Burton, M. J. Shashkov and P. P. Whalen, The construction of compatible hydrodynamics algorithms utilizing conservation of total energy, J. Comput. Phys., 146(1) (1998), 227–262.
[11] E. J. Caramana and M. J. Shashkov, Elimination of artificial grid distortion and hourglass-type motions by means of Lagrangian subzonal masses and pressures, J. Comput. Phys., 142(2) (1998), 521–561.
[12] E. J. Caramana, M. J. Shashkov and P. P. Whalen, Formulations of artificial viscosity for multidimensional shock wave computations, J. Comput. Phys., 144(1) (1998), 70–97.
[13] G. Carré, S. Delpino, B. Després and E. Labourasse, A cell-centered Lagrangian hydrodynamics scheme in arbitrary dimension, J. Comput. Phys., 228(14) (2009), 5160–5183.
[14] R. B. Christensen, Godunov methods on a staggered mesh-an improved artificial viscosity, Technical Report UCRL-JC-105269, Lawrence Livermore National Laboratory, 1990.
[15] B. Després and C. Mazeran, Lagrangian gas dynamics in two dimensions and Lagrangian systems, Arch. Rational Mech. Anal., 178 (2005), 327–372.
[16] J. K. Dukowicz, A general, non-iterative Riemann solver for Godunov's method, J. Comput. Phys., 61 (1985), 119–137.
[17] J. K. Dukowicz and B. Meltz, Vorticity errors in multidimensional Lagrangian codes, J. Comput. Phys., 99 (1992), 115–134.
[18] S. K. Godunov, A. Zabrodine, M. Ivanov, A. Kraiko and G. Prokopov, Résolution numérique des problèmes multidimensionnels de la dynamique des gaz, MIR, 1979.
[19] J. R. Kamm and F. X. Timmes, On efficient generation of numerically robust Sedov solutions, Technical Report LA-UR-07-2849, Los Alamos National Laboratory, 2007.
[20] V. F. Kuropatenko, On difference methods for the equations of hydrodynamics, in N. N.

Janenko, editor, Difference methods for solutions of problems of mathematical physics, Volume I, pages 116–149, Providence, RI, 1967. American Mathematical Society, Translated from the Proceedings of the Steklov Institute of Mathematics, No. 74 (in Russian) by J. M. Danskin.

[21] R. Loubère and E. J. Caramana, The force/work differencing of exceptional points in the discrete, compatible formulation of Lagrangian hydrodynamics, J. Comput. Phys., 216(1) (2006), 1–18.

[22] R. Loubère and M. J. Shashkov, A subcell remapping method on staggered polygonal grids for arbitrary-Lagrangian-Eulerian methods, J. Comput. Phys., 209(1) (2005), 105–138.

[23] G. Luttwak and J. Falcovitz, Slope limiting for vectors: a novel vector limiting algorithm, Conference on Numerical methods for multi-material fluid flows; Pavia University on September 21-25, 2009. Available at `www.eucentre.it/multimat09/media/presentazioni_congresso/luttwak.pdf`.

[24] G. Luttwak and J. Falcovitz, Staggered Mesh Godunov (SMG) schemes for ALE hydrodynamics, Numerical methods for multi-material fluid flows; St Catherine's College Oxford 5th-8th September 2005. Available at `www.icfd.reading.ac.uk/talks/Luttwak.ppt`.

[25] P.-H. Maire, A high-order cell-centered Lagrangian scheme for compressible fluid flows in two-dimensional cylindrical geometry, J. Comput. Phys., 228(18) (2009), 6882–6915.

[26] P.-H. Maire, A high-order cell-centered Lagrangian scheme for two-dimensional compressible fluid flows on unstructured mesh, J. Comput. Phys., 228(7) (2009), 2391–2425.

[27] P.-H. Maire, R. Abgrall, J. Breil and J. Ovadia, A cell-centered Lagrangian scheme for compressible flow problems, SIAM J. Sci. Comput., 29(4) (2007), 1781–1824.

[28] P.-H. Maire and B. Nkonga, Multi-scale Godunov-type method for cell-centered discrete Lagrangian hydrodynamics, J. Comput. Phys., 228(3) (2009), 799–821.

[29] L. Margolin, M. Shashkov and P. Smolarkiewicz, A discrete operator calculus for finite difference approximations, Comput. Meth. Appl. Mech. Eng., 187 (2000), 365–383.

[30] R. D. Richtmyer, Taylor instability in shock acceleration of compressible fluids, Commun. Pure Appl. Math., 13 (1960), 297–319.

[31] L. I. Sedov, Similarity and Dimensional Methods in Mechanics, Academic Press, New York, 1959.

[32] M. J. Shashkov, Conservative Finite-Difference Methods on General Grids, CRC Press, Boca Raton, FL, 1996.

[33] J. von Neumann and R. D. Richtmyer, A method for the numerical calculations of hydrodynamical shocks, J. Appl. Phys., 21 (1950), 232–238.

[34] M. L. Wilkins, Calculation of elastic plastic flow, in B. Alder, S. Fernbach and M. Rotenberg, editors, Methods in Computational Physics, volume 3, pp. 211–263, Academic Press, New York, 1964.

[35] M. L. Wilkins, Use of artificial viscosity in multidimensional fluid dynamic calculations, J. Comput. Phys., 36(3) (1980), 381–403.

[36] Y. Yang, Q. Zhang and D. H. Sharp, Small amplitude theory of Richtmyer-Meshkov instability, Phys. Fluids, 6(5) (1994), 1856–1873.